

**MODELING AND EXPERIMENTATION OF DRYING OF ADIPOSE DERIVED
ADULT STEM CELLS**

A Thesis

Submitted to the Graduate Faculty of the
Louisiana State University and
Agricultural and Mechanical College
in partial fulfillment of the
requirements for the degree of
Master of Science in Mechanical Engineering

in

The Department of Mechanical Engineering

by
Surbhi Mittal
B.Tech., S.C.T. College of Engineering, Trivandrum, 2001
December 2005

ACKNOWLEDGMENTS

It has been very rightly put forward by Johann Wolfgang Von Goethe, “Instruction does much, but encouragement does everything.” This has been true for me working with Dr. Ram Devireddy. His constant support, guidance, encouragement and motivation are the four pillars which have helped me to reach this point in my life. I will always be grateful to him for the technical insight, thought-provoking comments and optimism. I would like to extend my gratitude to Dr. Michael C. Murphy for many useful discussions on the use of ultrasound resonant sensors. I would like to immensely thank Dr. Dorel Moldovan for being on committee and the invaluable lessons I learnt during the curriculum.

My acknowledgements are also due to Dr. Gimble, Pennington Biomedical Research Centre for providing me the adult stem cells. At this point I would like to thank Dr. Yitshak Ram, Dr. Kumar Vikram Singh and Srinivas Gopal Krishna for the several fruitful discussions I had during modeling the resonant sensor.

A special note of thanks is also due to Aparna Prabhakar, Sreedhar Thirumala and all my lab-pals at Bioengineering Laboratory, Manu K. John and all my friends at LSU.

I would like to thank my parents, parents-in-law and sister for their constant words of encouragement, best wishes and prayers.

At this point I would like to thank my husband Dr. Nikhil Gupta for his constant support all through and being there at all times and without whom this work would not have been possible.

TABLE OF CONTENTS

ACKNOWLEDGMENTS	ii
LIST OF TABLES	v
LIST OF FIGURES	vi
ABSTRACT.....	viii
CHAPTER 1. PROBLEM DEFINITION AND LITERAURE REVIEW	1
1.1 INTRODUCTION - MOTIVATION FOR STUDY	1
1.2 PRESERVATION METHODS.....	3
1.3 ANHYDROBIOSIS	4
1.3.1 Examples from Nature	4
1.3.2 Experimental Studies	6
1.4 TREHALOSE: A MULTIFUNCTIONAL MOLECULE	15
1.4.1 Source of Energy and Carbon	15
1.4.2 Stabilization and Protection of Bilayers, Membranes, Proteins and Liposomes from Dehydration	16
1.4.2.1 Stabilization of Bilayers	16
1.4.2.2 Stabilizer of Phospholipids.....	16
1.4.2.3 Stabilizer of Dry Membranes	18
1.4.2.4 Stabilizer of Proteins	19
1.4.3 Protection against Heat	19
1.4.4 Protection from Damage by Oxygen Radicals.....	19
1.4.5 Protection from Cold and as a Growth Regulator.....	19
1.5 QUANTIFICATION OF WATER LOSS DURING DRYING.....	20
1.6 RESONANT SENSORS	22
1.6.1 Basic Principle and Physics of Resonant Sensors.....	22
1.6.2 Excitation and Detection Schemes.....	23
1.7 ALTERNATE EXCITATION AND DETECTION MECHANISM-ULTRASONICS	26
1.8 PROBLEM DEFINITION.....	29
1.9 OBJECTIVES OF THE CURRENT WORK	29
CHAPTER 2. DESICCATION OF ADULT STEM CELLS IN THE PRESENCE OF TREHALOSE AND GLYCEROL.....	31
2.1 INTRODUCTION	31
2.2 DESICCATION PROTOCOLS	33
2.2.1 Chemicals.....	33
2.2.2 Isolation, Collection and Culture of Adult Stem Cells	34
2.2.3 Addition of Trehalose and Glycerol.....	35
2.2.4 Convective Drying Stage	35
2.2.5 Assessment of Moisture Content in Dried Samples.....	36
2.2.6 Rehydration Protocol	36
2.2.7 Cell Membrane Integrity Measurements.....	37
2.3 STATISTICAL ANALYSIS	38

2.4	RESULTS	38
2.4.1	Choice of Drying Media.....	38
2.4.2	Convective Drying and Final Moisture Content	39
2.4.3	Effect of Drying Rate and Storage Condition on ASC Membrane Integrity	42
2.5	DISCUSSION	44
2.5.1	Anhydrobiosis and Choice of Drying Media	44
2.5.2	Intracellular Vs. Extracellular Trehalose	44
2.5.3	Concentration of Trehalose and Optimal Drying Conditions	45
2.6	CONCLUSION.....	48
CHAPTER 3. NUMERICAL INVESTIGATION OF THE PROPOSED SENSOR		49
3.1	MOTIVATION.....	49
3.2	MATHEMATICAL MODEL	50
3.2.1	Assumptions.....	50
3.3	DESIGN CONSTRAINTS	53
3.4	EFFECT OF BOUNDARY CONDITION ON THE FUNDAMENTAL FREQUENCY.....	54
3.5	OPTIMIZING THE DIMENSIONS OF THE VIBRATING BEAM.....	56
3.6	EFFECT OF MASS ON THE ULTRASONIC RESONANT SENSOR	59
3.6.1	Transcendental Eigenvalue Problem.....	60
3.6.2	Steps in Solving Transcendental Eigenvalue Problem Using Newton's Eigenvalue Iteration Method.....	62
3.7	EFFECT OF MASS ON THE FREQUENCY - USING TRANSCENDENTAL EIGENVALUE FORMULATION.....	64
3.8	FREQUENCY RESPONSE OF THE BEAM UNDER ULTRASONIC EXCITATION	71
3.9	PROCEDURE FOR ANALYZING FREQUENCY RESPONSE OF BEAM.....	71
3.10	EXTENSION OF THE BEAM MODEL TO A PLATE MODEL	76
3.11	CONCLUSIONS.....	80
CHAPTER 4. SUMMARY AND FUTURE WORK		82
REFERENCES.....		84
APPENDIX: TRANSCENDENTAL EIGENVALUE MATRICES		93
VITA.....		94

LIST OF TABLES

Table 1 Freeze Drying Studies Conducted on Prokaryotic Cells.	8
Table 2 Drying and Cryopreservation Studies Conducted on Plant and Animal Cells.	10
Table 3 Cryopreservation Studies Conducted on Mammalian Cells.	12
Table 4 Freeze Drying Studies Conducted on Mammalian Cells.	13
Table 5 A listing of studies conducted on the use of trehalose as a protective agent for drying storage of mammalian cells.	14
Table 6 Isolation and Culture of adipose-derived adult stem cells, Burt <i>et al</i> [80].	32
Table 7 Comparison of Average Cell Survival across Different Media.	39
Table 8 Data represented here are the means and standard errors of the means from 6 independent experiments for each passage using 50 mM Trehalose + 384 mM glycerol.	41
Table 9 Mechanical construction and the corresponding boundary condition.	52
Table 10 Material properties of Titanium.	53
Table 11 Value of non-dimensional parameter λ for different boundary conditions [120].	55
Table 12 Boundary Conditions for Beam 1 and 2 at the fixed ends.	65
Table 13 Four Continuity Conditions where the mass is loaded to maintain continuity.	65
Table 14 Weights of samples before and after drying.	67
Table 15 Fundamental Frequency Due to the presence of weight on the vibrating beam.	67
Table 16 Matching conditions including the effect of ultrasound.	72

LIST OF FIGURES

Figure 1 Some examples from nature for Anhydrobiosis (a) Brine Shrimp, (b) Tardigrade (c) Resurrection Plant.	5
Figure 2 Mechanism by which trehalose is thought to stabilize dry phospholipid bilayers, Crowe <i>et al</i> [9].	17
Figure 3 Schematic representation of an oscillator comprised of a resonator and a feed back loop.	23
Figure 4 Block diagram of the resonant sensor including a feed back loop along with the exciting and detecting mechanisms.	24
Figure 5 (a) A series and (b) a parallel resonant circuit.	27
Figure 6 Typical Ultrasonic System for Non Destructive Evaluation.	27
Figure 7 Adipose Derived Adult Stem cell expansion in culture along multiple lineage pathways, Burt <i>et al</i> [80].	32
Figure 8 Schematic of the Convective Drying Stage (not to scale).	37
Figure 9 Effect of media on desiccation tolerance.	39
Figure 10 Plot of weight fraction (represented as the ratio of the final to the initial weight) vs. time (min) for three different drying rates, in media containing D-PBS with 50 mM trehalose and 384 mM glycerol.	40
Figure 11 Dot plot of moisture content for P0 and P1 after various drying protocols: rapid (open circles), moderate (open squares) and slow (open triangles). All drying protocols carried out for 30min.	41
Figure 12 Comparison of the post rehydration membrane integrity across different flow rates.	43
Figure 13 Post Rehydration Membrane integrity for P0 and P1 after drying and storage at i) at ambient temperature, ii) in plastic bags, iii) vacuum sealed bags at ambient temperature.	43
Figure 14 (a) Beam in bending vibration, (b) Free-body diagram for a beam element.	52
Figure 15 Effect of beam length on the fundamental frequency of the beam under four different boundary conditions.	55
Figure 16 Variation of the fundamental frequency with length for different thickness.	58
Figure 17 (a) Axis Representation (b) Euler-Bernoulli beam (c) Violation of Euler-Bernoulli beam assumption by increasing the thickness.	58

Figure 18 Working range of thickness and length for the ultrasonic sensor.	59
Figure 19 (a) Schematic of mass on a beam (solving using transcendental eigenvalue problem) (b) free body diagram of the split beam.	64
Figure 20 Effect on the eigenvalue due to the presence of mass	67
Figure 21 Effect on fundamental frequency due to change in mass.	68
Figure 22 Effect of change in frequency with change in mass.	69
Figure 23 Frequency response of an unloaded beam.....	73
Figure 24 Shift in the resonant frequency is related to the change in mass.....	73
Figure 25 Shift in resonant frequency due to 20% change in mass.....	74
Figure 26 Shift in resonant frequency of the beam due to 60% change in mass.....	74
Figure 27 Shift in resonant frequency of the beam due to 90% change in mass.....	75
Figure 28 A linear relationship between the % change in the resonant frequency to the % change in mass brought about by drying.	75
Figure 29 Effect of variation in natural frequency for various aspect ratios of the plate.	77
Figure 30 Effect of variation of thickness on the fundamental frequency of the plate.....	78
Figure 31 Generalized graph relating the resonant frequency and dimensions of the vibrating plate.	79
Figure 32 Mode shape (1, 1) of the vibrating plate having aspect ratio of 8.....	80
Figure 33 Proposed experimental set up.....	83

ABSTRACT

Development of protocols for storing desiccated cells at ambient temperatures offers tremendous economic and practical advantages over traditional storage procedures such as cryopreservation and freeze-drying. An integrated frame work of experimentation and modeling is adopted in the present work to develop procedures for storage of adult stem cells at ambient temperature. As a first step, we have measured the post-rehydration membrane integrity of two passages, Passage-0 (P0) and Passage-1 (P1), of human adipose-derived stem cells (hASCs). hASCs were dried using a convective stage at three different drying rates (slow, moderate and rapid) in D-PBS with trehalose (50 mM) and glycerol (384 mM). After drying the ASCs were stored for 48 hrs, in three different conditions: i) at ambient temperature, ii) in plastic bags at ambient temperature and iii) in vacuum sealed plastic bags at ambient temperature. Post-rehydration membrane integrity was assessed after incubating the rehydrated ASCs. Also, the understanding of the entire drying procedure was extended by theoretically developing a novel ultrasound resonant sensor capable of quantifying the rate of water loss in real time. The sensor has been modeled as a conservative beam system and accounts for the effect on the fundamental frequency due to change in mass during drying when excited by ultrasound.

CHAPTER 1. PROBLEM DEFINITION AND LITERATURE REVIEW

1.1 Introduction - Motivation for Study

Stem cells are a class of undifferentiated cells that are found in the bone marrow, growing tissue or embryonic tissues. Stem cells include two essential characteristics (i) self renewal (indefinite cell division) and (ii) multipotency (differentiation into functionally distinct lineages) [1]. These types of cells have an immense potential in gene technologies for the use of living cells as therapeutic tools in clinical care [2]. This is because their extraordinary ability to multiply and divide indefinitely gives rise to specialized tissue or cell type by not only providing the starting material for organs but also for their continual growth, maintenance and repair.

Stem cells can be categorized into two distinct types: adult stem cells (ASCs) and embryonic stem cells. ASCs are defined depending upon the source from which they are derived. For example, hematopoietic stem cells are derived from bone marrow; neural stem cells are derived from central nervous system, hepatic stem cells that produce hepatocytes are found in liver [3]. On the other hand embryonic stem cells are derived from blastocysts and have a potential to differentiate to any cell type in the body. Recent findings have revealed that there is significant potential for producing novel cell-based products from stem cells. However, currently there are no effective technologically relevant methodologies for culturing stem cells outside the body, or for reproducibly stimulating them to differentiate into functional cells. It has been observed from recent studies [4] that similar multipotent stem cells also can be derived from tissues including dermis, skeletal muscle and adipose tissue. Unlike ASCs obtained from bone marrow or umbilical blood, which are relatively scarce, adipose derived adult stem cells can be recovered from liposuction “waste” material.

To maintain sufficient supply of ASCs for hospitals, medical centers and bio-medical research establishments it is essential to immediately develop long term storage methods [4]. Although there have been significant advances in the fundamental and practical level pertaining to cell and tissue culture differentiation and biomaterials, the tools needed for the storage of living cells lag significantly behind. Also, the developments in the pharmaceutical and biotechnology industries have led to the need for reliable stabilization and storage techniques for labile products, especially isolated proteins. Any biological product passes through successive operations between start and endpoint, i.e. they have to be shipped and stored at ambient temperatures (preferably), and rendered stable for reasonable periods. It has been observed that technical, therapeutic or commercial value of biological structures is measured by the biological or technological function they can perform per unit weight and in unit time, but some of the biological structures suffer rapid inactivation in dilute aqueous solution. However, destabilizing effects such as oxidation and denaturation; other chemical reactions can also cause substantial damage. It has been observed by Shalaev *et al* [5] that the methodology to improve long term stability can be achieved by sub-zero temperature storage (either frozen or unfrozen) and by drying. The concept of stabilization can be extended from applications of storing labile proteins to storing blood cells (platelets and erythrocytes) leading to a greater shelf life of human blood in the blood bank. In addition to this, effective procedures are also required to protect and conserve the endangered species of the world. The traditional programs of breeding and maintaining endangered species in captivity are not only difficult but also very expensive, thereby drastically limiting the genetic diversity of endangered species. Thus emphasis must now be placed on developing effective preservation methods. Some of the existing preservation methods are discussed below.

1.2 Preservation Methods

There are several effective preservation methodologies that can be used to preserve stem cells, sperm cells and the like. The current methodology for preserving species, organs and tissues involves creation of a state of “suspended animation”, known as cryopreservation. Cryopreservation is defined as a process where cells or whole tissues are stored at sub-zero temperatures, typically in the range of -80°C to -196°C . At low temperatures preservation occurs because any biological activities, including biochemical reactions that would eventually lead to cell death, are suspended or stopped [6]. The main limitations of cryopreservation protocols are the use of fairly complex methods, high concentrations of toxic cryoprotectants and costly freezing equipment that suffer from the inflexibility of storage requiring liquid nitrogen. Maintaining low temperatures initiates freezing injury. The freezing injury has been shown to have two components, direct damage from intracellular ice formation (IIF) and secondary damage caused by an increase in the solute concentration as progressively more ice is formed. A more recent approach for cryopreservation involves the use of low concentrations of intracellular sugars to stabilize cells. The major advantage of using nontoxic sugars is the prospect of infusing the freeze-thawed cells directly into patients without the cumbersome steps involved in the removal of traditional cryoprotectants.

Another method developed for the preservation of cells is Lyophilization or Freeze-Drying wherein the cells are suspended in a lyoprotectant. The lyoprotectant includes a macromolecule, which serves as a bulking agent and a disaccharide to protect the membrane [4]. A comparison between freeze-drying and cryopreservation reveals that cryopreservation is superior because it gives higher survival rates and is applicable to a wider range of tissue and cells.

To overcome the above stated hurdles associated with cryopreservation and freeze-drying, the recent focus is on the development of novel strategies to store living cells at ambient temperatures, which can be achieved by means of desiccation or drying. Preservation by desiccation is a method that attempts to replicate a naturally occurring preservation technique, namely *Anhydrobiosis* [7].

1.3 Anhydrobiosis

Nature has developed numerous strategies for the long term survival of organisms. The ability of living organisms to withstand damaging conditions like extremes of temperature, extreme cold, dryness and lack of oxygen is very thought provoking. Water is usually thought to be required for the living state, but numerous organisms are nevertheless capable of surviving near complete dehydration for long time periods. They commonly survive even when more than 99% of their body water is removed, which results in dry but viable tissues. This phenomenon known as *Anhydrobiosis*, challenges the fundamental precepts with regard to the role of water in the maintenance and promotion of life. Anhydrobiosis is achieved by a process involving a “reversible suspension” of the metabolism, which effectively isolates organisms from severe environmental changes. A thorough study on the response of microorganisms to stress environments has been carried out by Feofilova [8] and Crowe *et al* [9]. Anhydrobiotic engineering aims to confer a high degree of desiccation tolerance on otherwise sensitive living organisms and cells. How it works is still unresolved.

1.3.1 Examples from Nature

In nature, a variety of organisms including arctic frog, salamanders, tardigrades and nematodes, bacteria, yeast, fungi and rotifers survive extreme dehydration and dry conditions due to the presence of sugars as reviewed by Gundy [10] and Womersley [11]. Some of the examples from nature are shown in Figure 1. Morphological and behavioral adaptations are

apparent in some organisms experiencing water loss, for example the coiling and clumping exhibited by nematodes. These mechanisms are primarily thought of as a method to buy time to effect the biochemical changes which are actually responsible for the extreme biostability as observed by Perry [12]. An extensive study on common anhydrobiotic organisms has revealed that they undergo a series of complex adaptations to survive drying stress. Among these adaptations is the accumulation of internal sugars or mixtures of sugars, such as trehalose, sucrose and raffinose as represented in the study conducted by Crowe *et al* [13, 14].

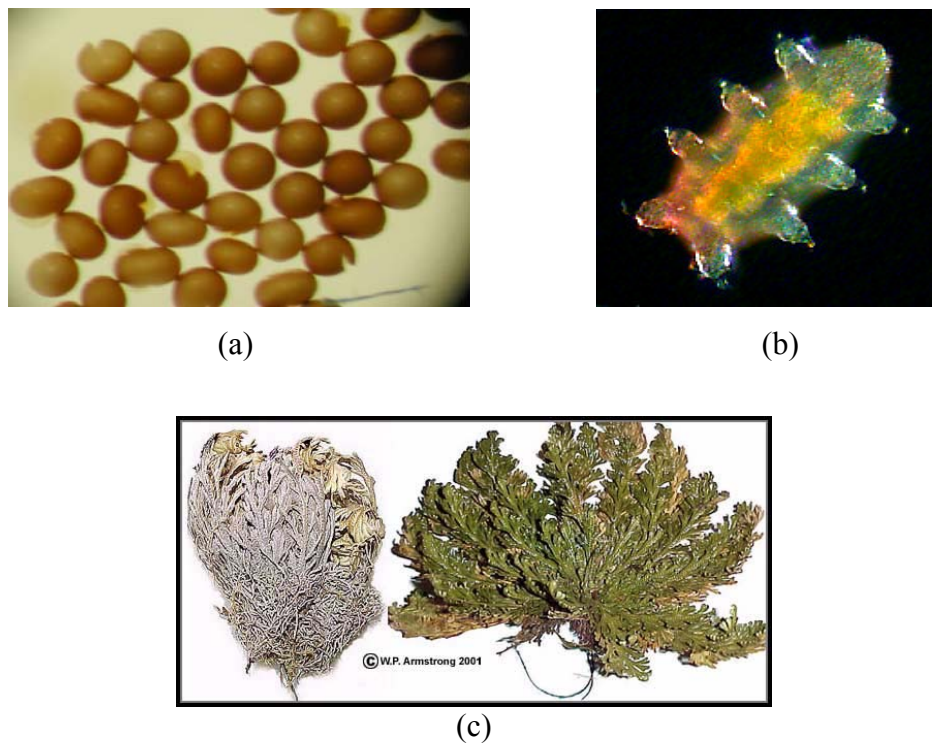


Figure 1 Some examples from nature for Anhydrobiosis (a) Brine Shrimp, (b) Tardigrade (c) Resurrection Plant.

1.3.2 Experimental Studies

The study of anhydrobiosis dates back to 1702 when Leeuwenhoek first described the recovery of live ‘animalcules’ from dried sediment from a roof top gutter as cited by Keilin [15].

On a molecular scale, the physical principles underlying the mechanism of damage from extreme dehydration are the same, regardless of whether the organism is an animal, microbe, or plant. It follows that the mechanisms by which the organisms escape that damage would be expected to share some common features such as accumulation of sugars. Studies conducted by Caffrey *et al* [16] have also suggested that the primary reason for preferring trehalose to sucrose is that the former molecule has lesser tendency to form crystals than that of sucrose. This was proved experimentally later by Green *et al* [17].

Studies on the drying preservation of both prokaryotes and eukaryotes have revealed that non-reducing sugars such as trehalose, sucrose, and maltose protect liposomes from the adverse effect of freeze-drying and drying [9, 18-20]. Desiccation studies carried out by Billi *et al* [21] and freeze-drying studies by Leslie *et al* [22] on *E. Coli* showed that addition of trehalose in the form of extracellular trehalose or sucrose to samples of *E. Coli* before freeze-drying or drying increased the overall viability of the samples. From these studies it is observed that some sugars like trehalose and sucrose protect not only the membranes but also intracellular proteins during a drying process. Similar results obtained by freeze-drying studies on *B. thuringiensis* [21] have supported the postulation that an increase in tolerance to drying appears to result from an ability of the sugars to lower the phase transition temperature of the membrane [23, 24]. Study by Brana *et al* [25] suggests that physiological changes that occurred in *Streptomyces antibioticus* revealed that this bacterium accumulated glycogen and trehalose during growth on solid medium. Glycogen storage in the substrate mycelium took place during development in aerial mycelium. The concentration of nitrogen source in the culture medium also influenced the time

at which the accumulation started as well as the maximum levels of polysaccharide stored. Trehalose was detected in all phases of colony development. Studies on *S. antibioticus* using electron and chemical microscopes were extended to understand the changes which the reserve compounds undergo in the course of development cycle. *Streptomyces antibioticus* bacterium, has a remarkable ability of growing and sporulating in air. Studied by Brana *et al* [26] revealed that their tolerance to extended drying periods may be due to trehalose:

- (i) initiating the growth cycle and serve as an energy source for germination or
- (ii) acting as an endogenous source of energy during the dormant period.

Similar freeze-drying studies, done on microbes by Miyamoto-Shinohara *et al* [27], reported that the survival remained the same even after long periods of about ~10 years when stored in vacuum. A study on the effects of trehalose on prokaryotic cells is given in Table 1. When the nematode *Aphelenchus avenae* was dehydrated slowly, it converted as much as 20% of its dry weight into trehalose molecule as studied by Madin *et al* [28]. In the absence of water the survival of these and other animals is also correlated with synthesis of the sugar. It has also been observed by Beker *et al* [29] that baker's yeast (*Saccharomyces cerevisiae*) accumulates trehalose, as intracellular trehalose, which appears to be required for survival of these cells and for other fungi and bacteria in the absence of water. Additionally, a study on the desiccation tolerance of *Saccharomyces cerevisiae* by Millie *et al* [30] reveals a positive influence on the survival and functionality when subjected to a mixture of glycerol and trehalose. The main aim of their work was to optimize a convective drying process for *S. cerevisiae* in which the sensitivity to osmotic stress and influence of the kinetics of dehydration in liquid medium (water-glycerol) are determined. It revealed that with the increase in the osmotic stress the viability decreased. With increase in the osmotic stress the final viability depends greatly on temperature.

Embryos of the brine shrimp, studied by Clegg [31], withstand removal of virtually all cellular water. Such embryos contain, in addition to trehalose, large quantities of a small heat-shock protein. This protein acts as a molecular chaperone *in vitro* and *in vivo* and has been shown to work synergistically with trehalose in inhibiting oxidation damage.

The damage to biological systems during drying is primarily due to the changes in the physical state of membrane lipids and changes in the structure of sensitive proteins. Desiccation tolerance has also been studied extensively in plant seeds. It is observed that a set of proteins, known as “late embryogenesis accumulating” (LEA), has a major role in protecting seeds from dehydration. Several varieties of plant species such as rice (*Oryza sativa*) and wild rice (*Zizania palustris*) have also been studied [32].

Table 1 Freeze Drying Studies Conducted on Prokaryotic Cells.

Cell Type	The type of study	Media	Assessment	Ref.
Intact Bacteria <i>E.Coli</i> and <i>B.thuringiensis</i>	Freeze Drying	A mixture of Trehalose and Sucrose (100mM each)	Membrane, Protein Structure- FTIR technique. 63% Highest Viability	22
Escherichia coli	Freeze Drying Air Drying Chemical Drying	Freeze drying in liquid nitrogen, Air drying under sterile air at room temperature, Chemical dried in nitrogen atm over phosphorus pentoxide. Rehydration by 10 or 100µl of sterile water, stored overnight.	Phase transition temperature measured by FTIR.	21
Microbes	Freeze Drying	No media specified. 10 different microorganisms were freeze dried and survival measured immediately and after 10 years.	CFU study. The survival rate was species specific. Bacteria, yeast behaved differently. Significant survival was observed in Yeast and bacteria.	27

In the study of soybean seeds by Blackman *et al* [33, 34] it was observed that high levels of both maturation proteins and oligosaccharides are necessary for the development of desiccation tolerance. The presence of maturation proteins is incapable of providing desiccation tolerance unless high levels of oligosaccharides, particularly stachyose for soybean, also accumulate. A study conducted on pedunculate oak (*Quercus robur*) [35] revealed that cryopreservation techniques based on vitrification significantly improved the survival. Several cryopreservation, freeze-drying and drying studies conducted on plant and animal species are listed in Table 2.

Extensive cryopreservation and freeze-drying studies have also been conducted on mammalian cells. As mentioned earlier traditional cryopreservation program uses high concentrations of sugars such as DMSO (~2M). A modification of this program involves microinjecting the mammalian cells with 0.2M of intra-and extracellular trehalose. Microinjection of trehalose was accomplished using gas-driven pico-injector [36]. A remarkable protection to the mammalian cells was observed even at low concentrations of trehalose during freezing. Additionally, a significant improvement in the survival was recorded when pancreatic cells, studied by Beattie *et al* [37], were frozen in a combination of trehalose and 2M DMSO.

Detailed studies on cryopreservation of mammalian cells in the presence of extracellular and intracellular trehalose were conducted revealing that the mere presence of trehalose in the media had a tremendous effect on viability (~80%). Intracellular trehalose was injected by porating the mammalian cells with α -hemolysin. Details of the various studies are represented in Table 3.

Viability studies on the mammalian cells using trehalose have been extended from cryopreservation to freeze-drying. Freeze-drying studies conducted on human platelets

Table 2 Drying and Cryopreservation Studies Conducted on Plant and Animal Cells.

Cell Type	The type of study	Media	Assessment	Ref
Saccharomyces cerevisiae	Air Drying Optimization	Convective Drying on Fluidized Bed Technology. Rehydration with water and glycerol (9 ml). Subjecting to different Osmotic Stress.	CO ₂ Release- System to measure dough extension, representative of the CO ₂ release. pH variation - in a computer controlled reactor.	30
Rice (<i>Oryza sativa</i>) Wild rice (<i>Zizania palustris</i>)	Drying	Dehydrated over saturated MgCl ₂ . Rehydrated in 100% RH for 24 hr.	Observed the accumulation of the dehydrin protein, ABA (Abscisic acid). ABA was detected by ELISA. Viability determined by Tetrazolium tests and Germination Tests. Seeds showed to be desiccation tolerant.	32
Soybean	Desiccation Tolerance	Dried -saturated LiCl solution, RH =13% at 25 °C. Rehydrated after 6 days for 24 hr in an atmosphere of high RH.	Observed the accumulation of heat stable proteins detected by SDS-PAGE analysis. ABA was also found to accumulate. Exogenous ABA (100µM) enhances the expression of Lea (late embryogenesis accumulating) protein.	33, 34
Barley Embryo	Desiccation Tolerance	Drying -by placing on 2 layers of filter paper in the constant stream of air in ventilating hood at 100°C.	Presence of 100µM ABA for desiccation tolerance. Conclusion that during embryo development the ability to germinate is acquired after a later stage than the ability to germinate precociously without drying.	38
Soybean	Glass Transitions Measurement	Effect of trehalose	ESR (Electron Spin Resonance) Presence of vitrification of the cytoplasm.	39

Table continued...

Cell Type	The type of study	Media	Assessment	Ref
Nematoda <i>Muellerius cf. capillaries</i>	Desiccation tolerance	RH was controlled in sealed desiccators. K ₂ SO ₄ for 97% RH, MgCl ₂ .6H ₂ O for 33% RH, fresh silica gel for 0% RH.	Determined by monitoring the larval motility over a 24hr period and compared for different RH regimes. Sustained rapid dehydration stress for short periods and at slow rates of water loss.	40
Nematodes <i>Aphelenchus avenae</i>	Metabolism study during anhydrobiosis	Pellets of the sample dried at 97% RH, after which pellets placed in air over CaCl ₂ for 24-48 hr.	Anhydrobiotic worms prehydrated at 97% RH and placed in water in Respirometer. Functionality checked by the oxygen uptake. Observed-anhydrobiotic worms synthesize glycogen and degrade trehalose, glycerol and lipids.	28
<i>Quercus robur</i> (Oak)	Cryopreservation after Desiccation Vitrification	300 mM sucrose and 700 mM sucrose for 4 days air dried in laminar flow cabinet for 0-4 hr, cooled. Vitrification Medium: 300mM of sucrose. Then cooled	Higher desiccation time lower viability Reduced to 15-20%. Sucrose further assisted in the cryopreservation process after the drying process. Recovery rates high ~ 70- 90% after cryopreservation.	35

Table 3 Cryopreservation Studies Conducted on Mammalian Cells.

Cell Type	Media	Assessment	Ref.
Human Oocytes	No Trehalose, Extracellular Trehalose 500 mM Intracellular Trehalose 150 mM intra-and 500 mM extracellular trehalose.	Membrane Integrity measured for different cooling rates.	36
Mammalian Cells Fibroblasts	200 mM trehalose.*	Flow Cytometry, 80% viability	42
Mammalian Cells keratinocytes	200 mM extracellular trehalose.	The presence of trehalose significantly improved the survival rate to 43%. Flow Cytometry	
Goat Sperm Membrane	Trehalose 375 mM or different combinations of trehalose with glucose.	Higher sperm motility with high concentrations of Trehalose. Increase in post that motility with increase in % of trehalose increase. Fluidity study performed by FTIR.	43
Hematopoietic Cell Line	Loading with 200 mM, freezing and then viability check.*	Cell poration efficiency: with out Trehalose-42-62% with trehalose 87%. Colony formation (CFU) study Flow cytometric analysis.	44

*intracellular Trehalose (using α -hemolysin)

by Wolkers *et al* [41] revealed that an efficient methodology for the uptake of trehalose is simple incubation at 37°C. Similar freeze-drying studies have been performed on stem cells using low concentrations of intracellular trehalose, with the difference that the trehalose was infused into the stem cells using the porating agent α -hemolysin. A comprehensive listing of freeze-drying study on mammalian cells is represented in Table 4.

The need to store stem cells and other mammalian cells in ambient temperature has led to several desiccation related studies, some of which are listed in Table 5. Each of these studies emphasized on optimizing the trehalose concentration to achieve maximum post-drying

membrane integrity. It has been noted that trehalose concentrations above 200 mM led to cytotoxicity and concentrations below 50 mM resulted in a considerable decrease in viability. Final viability conducted by such desiccation studies also depended on the mode of storage.

Table 4 Freeze Drying Studies Conducted on Mammalian Cells.

Cell Type	The type of study	Media	Assessment	Ref.
Mouse Oocyte	Osmotic Stress study in presence of intracellular sugars	Oocytes microinjected with 800 mM glucose, trehalose solutions for intracellular concentration of 100 mM, expose to hypertonic solutions with increasing strength 200, 300, 500 and 700 mM	Volumetric changes as a result of exposure to different osmolalities by image processing program and the by the Boyle, vant Hoff plot. Osmotic behavior of mouse zygote was similar in different external mono- and disaccharide solutions.	46
Human Platelets	Freezing and Freeze Drying	350 mM Trehalose. Rehydrated with 1 ml PBS solution.	Morphology by a standard microscope. Optical Density of freeze dried cells - absorbance spectrometer. Prehydration increases viability.	41, 47
	Freeze Drying	Incubated in 35 mM Trehalose. Rehydration in a closed box with moisture-saturated air at 37°C.	Platelet count-measured using Coulter T890 counter before drying and rehydration. Morphology- standard light microscope. Membrane fluidity measured -FTIR.	
Mouse Spermatozoa	Freezing, Freeze-Drying without Cryoprotectants	Sperm injected oocyte and embryos cultured in CZB medium supplemented with 5.56 mM glucose.	Fertilization spermatozoa without cryopreservation 89%, freeze dried spermatozoa 68% and after ICSI of the spermatozoa 96%.	48
Kidney Cells	Effect of Trehalose	Kidney cell line transfected with pCMV	HPLC measurement for trehalose concentration. Gradual decline of viability is measured over the days.	49

Table 5 A listing of studies conducted on the use of trehalose as a protective agent for drying storage of mammalian cells.

Cell Type	Media	Post-Storage Assessment	Observations (optimal conditions)	Ref.
Human Primary Foreskin Fibroblasts	Biosynthesis of trehalose	Viability (membrane integrity)	Vacuum storage and 50 mM trehalose is optimal. Less than 150 mM trehalose induces cytotoxicity.	49
3T3 Murine Fibroblasts*	0 to 400 mM trehalose	Viability (membrane integrity)	Membrane integrity decreases with moisture content. Greater integrity when stored at 4°C and -20°C.	50
Human Mesenchymal Stem Cells (hMSCs)	50 mM trehalose + 3% glycerol (incubated 24 hr before drying)	Morphology; Adhesion; Viability; Proliferation.	Vacuum storage and incubating with trehalose before drying improved desiccation tolerance.	51
3T3 Fibroblasts*	200 mM intra- and extracellular trehalose	Viability (membrane integrity)	10% residual moisture; natural convection; initial osmolality of the sugar solutions adjusted to isotonic levels by reducing buffer concentration.	52
Human Corneal Epithelial Cells	2 to 200 mM of either trehalose or maltose.	Viability (membrane integrity);	< 20 mM trehalose not useful; maltose had no effect.	53
Mouse Spermatozoa*	500 mM trehalose	Blastocyst formation	Desiccated in ambient temperature with 500mM of trehalose, stored at 4°C.	54

*intracellular Trehalose (using α -hemolysin)

Several other important findings that affect the final cell viability can be related to drying conditions which directly or indirectly affects the moisture content (although not clearly stated), the temperature at which drying was conducted, the osmolality of the surrounding medium and mode of transfecting trehalose into the cells.

1.4 Trehalose: A Multifunctional Molecule

From the extensive literature presented it is evident that a single perturbation in the cell system results in synthesis of trehalose, which in turn leads to considerable tolerance of plant, animal and mammalian cells towards desiccation. It is also observed that the biosynthesis and hydrolysis of trehalose extends the understanding of its functions in cells and its significance on homeostasis on organisms that produce it [45].

A deep understanding of the structure and functions of trehalose is mandatory to understand how it aids in the desiccation tolerance. Trehalose is a nonreducing disaccharide of glucose and structurally it contains two glucose units, which are linked in an α , α -1-1-glycosidic linkage. It is found that this molecule is a source of energy and carbon in a wide variety of organisms, including bacteria, yeast, fungi invertebrates, and lower and higher plants. It has also been shown that trehalose can protect proteins and cellular membranes from inactivation and denaturation caused by a variety of stress conditions including desiccation, dehydration, heat, cold and oxidation. Trehalose can perform a variety of functions, a few of which are discussed below.

1.4.1 Source of Energy and Carbon

The amount and level of trehalose varies greatly in certain cells depending upon the state of growth of the organism or cell and environmental conditions. Studies conducted by Becker *et al* [55] revealed that trehalose, present in the thorax muscles of insects, is consumed during flight

thus acting as a source of energy. Trehalose also plays an important role in the germinations of the fungal spores by serving as a source of carbon for synthesis and glucose for energy.

1.4.2 Stabilization and Protection of Bilayers, Membranes, Proteins and Liposomes from Dehydration

1.4.2.1 Stabilization of Bilayers

The two primary stresses that are known to destabilize lipid bilayers during dehydration are fusion and lipid phase transitions. Light scattering techniques demonstrate that trehalose inhibits fusion between vesicles during drying while the x-ray diffraction studies reveal that trehalose fits well between the polar head groups of the membrane with multiple sites of interaction. The strong stabilization effects of trehalose can be related to its stereochemistry, which provides the most favorable fit with the polar head groups, hence stabilizes the bilayers.

1.4.2.2 Stabilizer of Phospholipids

An extensive study conducted by Crowe *et al* [9] revealed the mechanism by which trehalose protects the phospholipids during drying. Membrane phospholipids are hydrated, particularly in the case of phosphatidylcholine, where 10-12 water molecules are hydrogen bonded around each phosphate accounting for 20% of the weight of the hydrated bilayer. When the water is removed the packing of the head group increases, leading to an increase in Van der Waal's interaction among the hydrocarbon chains. This results in an considerable increase in the phase transition temperature. Thus the dry lipids would be in gel phase at room temperature. As a result when the lipids are placed in water or hydrated it is expected that they would undergo a phase transition. It is important to note that as the membranes pass through the phase transitions they become leaky, which can prove to be deleterious. This effect is more pronounced when the dry bilayer in gel phase is rehydrated. There is substantial evidence suggesting that trehalose prevents this leakage by depressing the phase transition temperature (T_m) of the dry lipids

maintaining them in liquid crystalline phase in the absence of water as illustrated in Figure 2 [9]. Here, the role of trehalose is to depress the T_m well below that of the fully hydrated lipids. Depression of T_m by trehalose is strongly correlated with retention of the trapped solute. As a result of this effect, the dry lipids do not undergo a transition from gel to liquid crystalline phase during rehydration and do not leak. This mechanism is represented schematically in Figure 2. Also, an underlying mechanism of interaction with phospholipids has been established. It is stated by Crowe *et al* [56-58] that the stabilizing effect of trehalose on phospholipids bilayers is the result of direct interaction between -OH groups on trehalose and the phosphate of the membrane phospholipids. This is basis of the *water replacement hypothesis*, which suggests that during drying, sugars substitute water molecules (in particular by forming hydrogen bonds) around the polar and charged groups present in the phospholipids membranes and proteins, thereby stabilizing the native structure in the absence of water [59, 60].

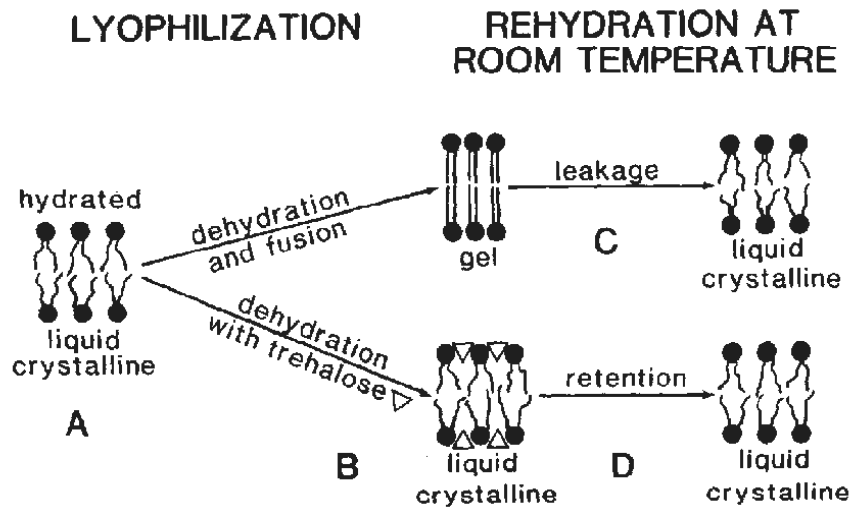


Figure 2 Mechanism by which trehalose is thought to stabilize dry phospholipid bilayers, Crowe *et al* [9].

1.4.2.3 Stabilizer of Dry Membranes

When liposomes were dried with trehalose and then rehydrated, vesicles that retained almost 100% of original contents were obtained whereas those dried without trehalose leaked all of their contents during drying and rehydration. To quantify the extent of fusion, resonance energy transfer between fluorescent probes incorporated into the bilayer was studied, which revealed that trehalose was sufficient in inhibiting fusion. In the case of membranes, trehalose probably interacts directly with the dry protein by hydrogen bonding between its hydroxyl groups and the polar residues in the protein [61]. To extend this argument of trehalose stabilizing dry membranes, investigations on Sarcoplasmic reticulum isolated from muscle was studied. This served as a model membrane to study the effects of desiccation, Crowe *et al* [56]. The initial (pre-desiccation) morphology and functionality of these membranes were as seen in freeze fracture studies and transport of Ca^{++} respectively. Drying in the absence of trehalose revealed that the vesicles fused i.e. their morphology altered and upon rehydration it was observed that all Ca^{++} -transport capacity was lost. However, when the membranes were dried with trehalose at concentrations near those found in anhydrobiotic organisms, morphological damage was completely inhibited during drying and upon rehydration vesicles were obtained that transported Ca^{++} at rates similar to those seen in freshly prepared vesicles.

The dry vesicles may be stored for over six months without loss of stability, as long as they are protected from oxygen [62]. This phenomenon of stabilization forms the basis of the water entrapment hypothesis, which proposes that sugars concentrate residual water molecules close to the biostructure, thereby preserving to a large extent its solvation and native properties [59].

1.4.2.4 Stabilizer of Proteins

Even though the mechanism of stabilization of proteins by interaction with trehalose has not been established, studies reveal that trehalose being a non reducing sugar cannot undergo the damaging browning reaction that usually occurs between the aldehyde group on a reducing sugar and the amino group in proteins. This could be due to the fact that sugars found in anhydrobiotic organisms, known to be good vitrifying agents, protect biostructures through the formation of amorphous glasses, thereby reducing structural fluctuations and preventing denaturation or mechanical disruption of proteins [59, 63].

1.4.3 Protection against Heat

An important *in vivo* and *in vitro* study conducted suggested that trehalose protects cells from heat by stabilizing proteins at high temperatures. Investigations performed with the help of certain temperature sensitive reporter genes showed that enzymes are able to retain their activity during heat shock in cells that are producing trehalose. The additional role trehalose plays, is the ability to suppress aggregation of proteins that have been denatured [45].

1.4.4 Protection from Damage by Oxygen Radicals

Another vital role played by trehalose is in protecting cells against oxygen radicals. It has been observed that trehalose acts like a free radical scavenger. Effects of other sugars such as mannitol and galactose have also been evaluated and it was observed that these sugars protect less than trehalose whereas sucrose was ineffective.

1.4.5 Protection from Cold and as a Growth Regulator

Trehalose may also stabilize cell membranes whose fluidity decreases with temperature decrease. Exogenous trehalose has been shown to protect a variety of organisms during freezing wherein the maximum protection is observed when trehalose is present on either side of the membrane. Some researchers have also postulated that trehalose or related metabolites might

function as regulators of plant growth and development as studied in tobacco plant. It has also been revealed that this phenomenon does not occur in mammalian cells. However, the traces of trehalose metabolism are found in kidney and in the intestinal villae membranes. Though its role in kidney is not yet established but it has been observed that it hydrolyzes the ingested trehalose [45]. Individuals with the defect of internal trehalase have diarrhea when food containing high percentage of trehalose (like mushrooms) is ingested. Thus, from the studies it has been observed that trehalose can be postulated as an ideal cryoprotectant for membranes and intact cells. It is also determined that many molecules have cryoprotectant properties but only a few protect against dehydration damage and trehalose is among them. It is regarded as a compatible solute that stabilizes biological structures in bulk solution.

A distinct feature that lacks considerably in all these studies is a mode to quantify the water loss during drying performed by natural or forced convection process. Once the rate of water loss from any cellular suspension is determined, it is expected that a better correlation between the viability and final moisture content can be established, which will further optimize the biopreservation protocol achieved by desiccation.

1.5 Quantification of Water Loss During Drying

A general consensus now exists that stability can best be achieved in the solid state and stabilization is equated to drying. In principle, crystallization should then be the preferred method because a crystal is the thermodynamically stable solid state. A better understanding of achieving the stable state of the loss of moisture during drying has to be developed. Micro and nanoelectromechanical systems represent an emerging sensor technology that provides a closely coupled link between the physical, chemical and biological worlds. Such system can be used as mass sensors with a sensitivity several orders of magnitude better than conventional oscillators. In the published literature the methodology adopted for measuring the loss of moisture/water

from the biological suspension is Gravimetric Analysis. In this procedure the percentage of moisture is calculated by the relation represented in Equation (1)

$$\text{moisture \%} = \left(\frac{\text{dried weight} - \text{baked weight}}{\text{wet weight} - \text{baked weight}} \right) \times 100 \quad (1)$$

where the wet weight is the starting weight of the sample; baked weight is the weight after an equivalent sample has been heated overnight at 90°C for 24 h in an oven; and the dry weight is the weight of the sample after the drying protocol has been completed [64, 65]. The calculation of moisture percentage in the above stated methods is based on the assumption that the baked weight is entirely free of moisture. In order to optimize the biopreservation protocol by desiccation understanding of the moisture loss becomes important. A probable solution is proposed by entering the realm of *Sensors*. Previous methods employed in the field of sensing of molecular binding [66, 67] chemical reactions and specific biomolecular interactions have been based on static deflection of microfabricated cantilever beams [68, 69]. Through various detection mechanisms [70] the mechanical signal can be transduced into either an optical or electrical signal and can be correlated to the change in mass on the vibrating structure. Alternative approach for detection is based on dynamic interrogation utilizing resonant mechanical sensors [71]. Studies have revealed that bulk acoustic-wave resonant piezo-layers (RPL) made of lead zirconate titanate (PZT) [72] on alumina substrate are sensitive to added mass and are used for gravimetric chemical sensing. Most of the models developed to this end are based on the following assumptions:

- (i) Resonator lateral dimensions are indefinitely large and the wave propagation is assumed to be purely planar along thickness.
- (ii) The boundary effects are neglected.

(iii) A loss-free system is assumed, not taking into account the dissipative effects.

1.6 Resonant Sensors

Resonant Sensors are frequency output sensors. In a resonant sensor the measurand affects the characteristic of the oscillation of a solid structure. In most of the resonant sensors the resonant frequency is altered and also the vibration amplitude. The phase and the damping i.e. the quality factor of the resonance are available as read out parameters. Since, these are primarily frequency output sensors they have the following advantages:

1. The digital output signal can be connected directly to digital signal processing electronics. This class of sensors has a very large dynamic range.
2. The dynamic range can be further increases by increasing the measurement time.
3. High Accuracy.
4. Good repeatability.
5. Low Hysteresis.

These properties are dependent on the sensor design and not on the type of the output signal.

1.6.1 Basic Principle and Physics of Resonant Sensors

The vibrating element in a resonant sensor can have any geometrical configuration. It can be beam, plate, membrane or a diaphragm. Hence, these shapes can have different vibration, e.g. transversal, torsional and lateral. Considering them as a distribute mass and spring system an infinite degrees of freedom is possible, hence, an infinite number of resonances or vibrational modes is possible for every type of vibration. A resonant sensor is designed in such a way that one of the modes dominates and the resonant frequency is made dependent on the measurand by letting the measurand change the stress, mass or shape of the resonator [73]. Resonant Sensors have potential application for precision measurement of mechanical quantities such as force, pressure, acceleration and flow. The most outstanding advantage of such resonant sensors is that

the stress-sensitivity can be made much larger than that of piezoresistive strain gauges and since the output is frequency it can easily be interfaced with digital equipment [74, 75]. In literature on resonant sensors, the measurand is nearly always considered being changed quasistatically, that is a steady state solution of equation is considered. This approach is justified with a slowly changing measurand. Usually the mechanical resonator is a part of the larger system which also contains one or more elements for excitation and detection. An electronic feed back circuit can be incorporated in the system to maintain the system in oscillation as shown in Figure 3.

1.6.2 Excitation and Detection Schemes

The resonant sensor consists of a resonator structure and components to excite and detect the mechanical vibrations. Figure 4 illustrates the different components of a resonant sensor in a block diagram. In a resonant sensing system an amplifying feedback loop can be incorporated between the exciting and the detecting systems to operate the resonator continuously at the fundamental resonance frequency. This helps in continuously monitoring the measurand. This

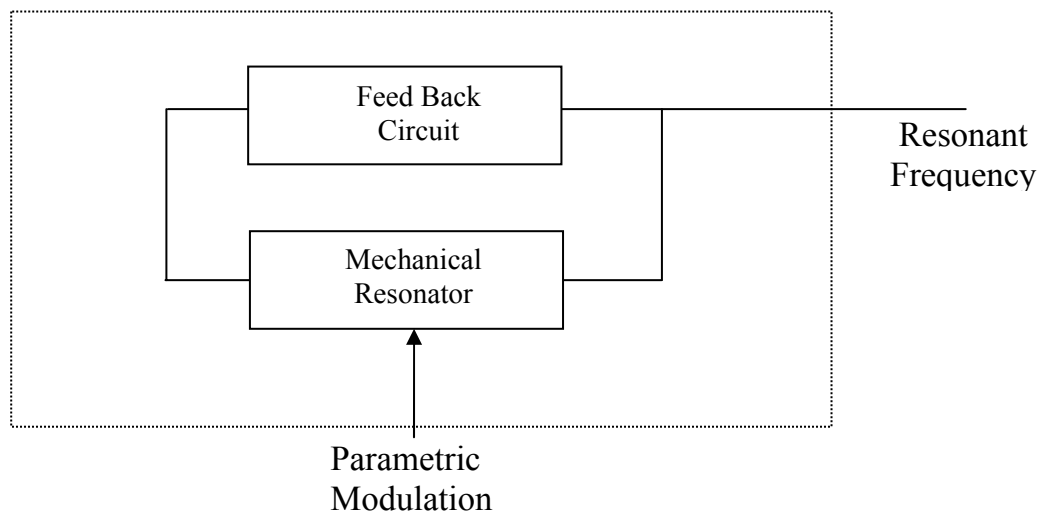


Figure 3 Schematic representation of an oscillator comprised of a resonator and a feed back loop.

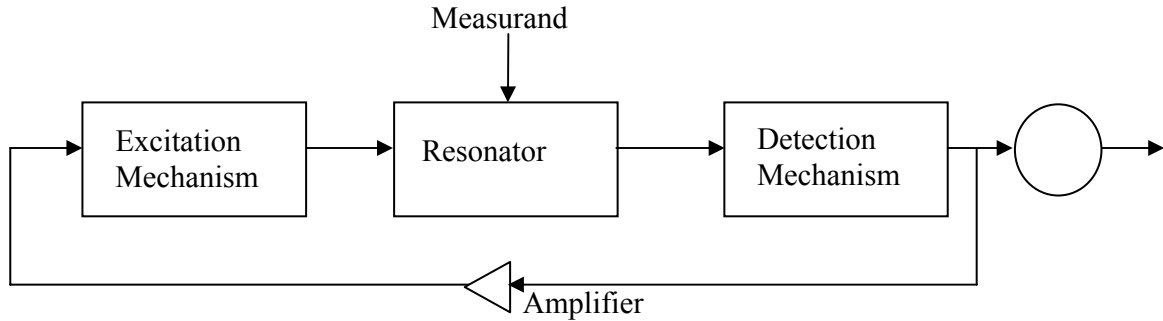


Figure 4 Block diagram of the resonant sensor including a feed back loop along with the exciting and detecting mechanisms.

principle takes advantage of the bandpass characteristic of the resonant structure itself and requires relatively large quality factors to obtain sufficient short term frequency stability. An amplifying feedback loop is commonly employed in the resonant sensor design if the resonance frequency is the output of interest.

Resonant sensors have wide spread applications. Compared to the traditional chemical microsensors without moving parts, microcantilevers present some interesting properties such as good sensitivity and compactness. In this type of sensors two principal modifications of the sensors are utilized, one resulting from variation of the resonant frequency resulting from the mass modification of the system or the bending variation due to the difference in mechanical surface stress induced in the system [76, 77].

Many different excitation and detection mechanisms for micromechanical resonators have been investigated, which are based on excitations of electrostatic, piezoelectric, electromagnetic and electrothermal and optothermal nature.

Electrostatic excitation and capacitive detection is accomplished by the attracting force between two capacitor plates, one being the resonator and the other being the substrate. Capacitive detection is based on the fact that a charged capacitor causes a change in the current if

the capacitance fluctuates. For a high Q-factor to be achieved the entire process has to operate in vacuum, which is cumbersome. Another problem is that small capacitance changes produces small current values which results in a very small detection signal, which necessitates large amplification.

Magnetic excitation and detection is easily realized with the help of an external magnetic field. An electric current flowing through a microbridge results in a Lorentz force which is the underlying principle for magnetic based resonators. Usually an H-shaped resonator is used where one beam of the H is used for excitation and the other for detection based on the principle of magnetic induction. If low doped silicon is used to fabricate the microbridges, transduction can be achieved without spoiling the superior material properties of single crystalline silicon by the deposition of thin films. The disadvantage of this type of sensors is that signals are very small and it is difficult to integrate a magnet in the sensor. Besides, the heat dissipated by conducting a current through the microbridge can cause compressive stresses due to thermal expansion.

Piezoelectric excitation and detection using quartz resonators is the most widely used method, exploiting the piezoelectric property of quartz. To make such devices compatible with silicon based devices, other materials have to be used, preferably in the form of thin films. The most commonly used material is ZnO which is sputtered on the quartz crystal. A problem with sputtering ZnO is that it is sensitive to humidity and light and has a history of thermal treatment that is not IC compatible. Deposition of ZnO also considerably reduces the quality factor and increases temperature sensitivity due to differences in thermal expansion.

Electrothermal excitation and piezoresistive detection are easily achieved. The two transduction mechanisms form a pair because both can be produced using the same material (doped polysilicon thin films) in the processing steps. The excitation mechanism is based on

thermal expansion. A heat source can give rise to a temperature gradient across the whole beam. If the thermal wave produced in the beam is of the order of the thickness of the beam or larger then the bending moment is independent of the frequency, else if the penetration depth is smaller than the thickness then the bending moment is inversely proportional to the frequency. This applies for high frequencies. Disadvantages associated with such excitation and detection mechanism is that the thermal stresses produced in the microbridge can cause it to buckle. Even if buckling can be avoided the thermal stresses have to be very well controlled. This causes problems associated with the performance of the sensor. Electrothermal excitation is very useful for sensors which explicitly use thermal domain.

Optothermal excitation and optical detection is another mechanism for exciting sensors at their resonant frequency. This technique provides an important advantage of the possibility of avoiding any electrical contact. The excitation mechanism is similar to the electrothermal excitation with the difference that the heat source is provided by the absorption of light. For optical detection methods, such as variation of transmission through a gap in a wave guide by means of a shutter using an optical proximity sensor or by integrated interferometry are utilized. Dielectric excitation is based on the lateral deformation of a dielectric thin film, sandwiched between two electrodes. Changes in deformation cause a change in the bending moment and the detection is capacitive, based on the change of the capacitance of a dielectric capacitor if the dielectric is deformed. The mechanical resonance in such circuits can be modeled electrically by a series resonant circuit or a parallel resonant circuit as shown in Figure 5.

1.7 Alternate Excitation and Detection Mechanism-Ultrasonics

Ultrasonics use frequencies higher than that of sound for conducting examinations and making measurements. The applications of ultrasonics is wide spread, it can be used for flaw detection/evaluation, material characterization, dimensional measurements and more. The

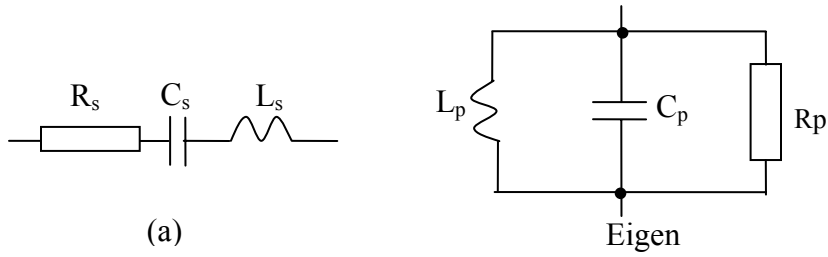


Figure 5 (a) A series and (b) a parallel resonant circuit.

operating procedure of a typical pulse/echo configuration used for flaw detection in materials is illustrated in Figure 6. The focus of ultrasound in vibrations is not in understanding the vibrational motion that occurs at the atomic level. The phenomenon of oscillatory motion arises when the particles are displaced from the equilibrium position. Due to this displacement from equilibrium position internal restoration forces arise which leads to oscillation.

In solids waves propagate in four principal modes and are based on how the particles vibrate. They can be classified as longitudinal, shear, surface and plate waves. The velocity of

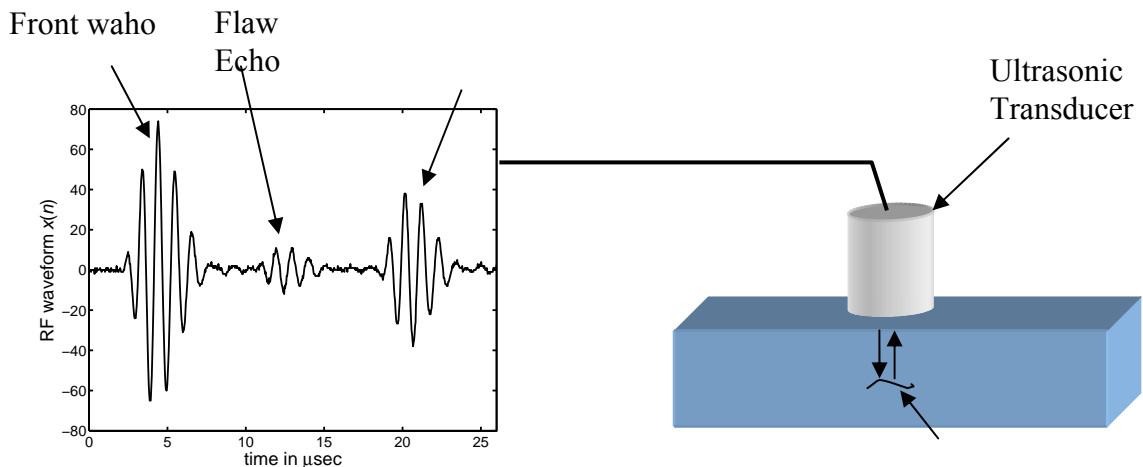


Figure 6 Typical Ultrasonic System for Non Destructive Evaluation.

sound in long slender bar in which the particle motion is parallel to the axis of the bar is termed as longitudinal velocity. The longitudinal thin bar velocity is given by Equation (2)

$$c_0 = \left(\frac{Y}{\rho} \right)^{1/2} \quad (2)$$

where Y is the young's modulus of elasticity, ρ is the density of the bar and c_0 is the velocity. When the particle motion in the wave is normal to the direction of propagation, the energy passes from one element to the other by shear stresses and the wave is called shear wave. While considering the shear wave, the shear modulus, μ , is a factor in the velocity represented in Equation (3).

$$c_s = c_0 [2(1 + \sigma)]^{-1/2} = \left(\frac{\mu}{\rho} \right)^{1/2} \quad (3)$$

Some ultrasonic waves follow the contour of the surface of a medium and penetrate the medium only at shallow depths. These waves are known as surface waves. There are two types of surface waves, Love waves and Rayleigh waves. The particle motion in Love waves is normal to the direction of propagation and polarized in the plane of the surface. Rayleigh waves are normal to the surface and particle motion is elliptical. When a plane wave encounters a plate that is very thin relative to the wave length, the plate flexes with the wave. In this mechanism it is considered that the pressures on the two faces of the plate are approximately equal in magnitude. It has been also studied that if the medium on both sides of the plate are same then the intensity of the transmitted beam approximately equals the intensity of the incident beam. Interference of the waves from the back surface of the plate occur if the plate thickness is of the same order as that of the wavelength in the plate, if the plate is one quarter wavelength thick then the reflections are 180° out of phase with the incident wave and no energy is transmitted under

such conditions. If the plate is one-half the wavelength thick, transmission is the maximum and only losses associated with attenuation are encountered. The relative transmission is given by Equation (4)

$$\frac{I_T}{I_I} = \frac{e^{-2\alpha d}}{\left[1 + \frac{1}{4} \left(\frac{Z_2}{Z_1} - \frac{Z_1}{Z_2} \right)^2 \sin^2 \frac{\omega d}{c_2} \right]} \quad (4)$$

where, Z_1 , Z_2 are the acoustic impedances of the surrounding medium and the plate respectively, d is the thickness of the plate, α the angle of incidence, c_2 is the velocity of sound in the media.

The review of existing studies reveals that considerable amount of work needs to be done in order to successfully achieve desiccation and storage of ASCs at ambient temperature. The theoretical and experimental studies need to be carried out to develop desiccation protocols, instrumentation and technology to ascertain the long term viability of ASCs.

1.8 Problem Definition

Existing techniques of desiccation use a convective drying stage, an approach that has advantages in terms of cost as well as ease of use. The focus of the present study is to adapt the convective drying technique to desiccate Adipose Derived Adult Stem Cells (ASCs) in the presence of extracellular sugars thereby creating cellular preparations that are shelf-stable and storable at ambient temperatures.

1.9 Objectives of the Current Work

In a complex and natural phenomenon known as anhydrobiosis, it is expected to have a myriad of events required for survival from drying. Extensive literature review shows that a single perturbation i.e., synthesis of a disaccharide such as trehalose is sufficient to achieve survival. Thus, with certain adaptations the survival can be enhanced from a short duration to a

longer one. Also, with the development of micromechanical sensors the biopreservation protocol by drying can be optimized. The objectives of this work primarily are

1. To develop a drying protocol for the successful desiccation and storage of ASCs at ambient temperature.
2. To validate the developed desiccation protocol through extensive drying experiments and perform post rehydration membrane integrity test of ASCs to optimize the drying and storage conditions.
3. To develop an analytical model of a microplatform to quantify the water loss during drying when excited by ultrasound and detect the change in mass by correlating it with the change in the resonant frequency of the microplatform.

CHAPTER 2. DESICCATION OF ADULT STEM CELLS IN THE PRESENCE OF TREHALOSE AND GLYCEROL

2.1 Introduction

Adult stem cells (ASCs) have traditionally been used to refer to the hematopoietic progenitors isolated from bone marrow and transplanted into patients after high dose of chemotherapy. With time there has been a radical shift in the concept of ASCs [78]. Firstly, recent evidence suggests that transplanted bone marrow-derived hematopoietic stem cells not only differentiate along hematopoietic pathways, but are also found as mature cells in the skin, brain, muscle, intestinal epithelium and liver of recipients. Secondly, it has been observed that bone marrow derived stromal cells are multipotent. Bone marrow-derived stromal cells differentiate along osteoblast, adipocyte, cardiac, myocyte, neuronal, and other pathways. It is now accepted that these ASCs display a wide range of plasticity that extends across traditional embryologic dermal boundaries [78]. Similar multipotent stem cells have been derived from other adult tissues including dermis [79], skeletal muscle and adipose tissue. Human adipose tissue provides a uniquely abundant and accessible source of ASCs [80]. In response to chemical, hormonal or structural stimuli, these adipose derived ASCs can differentiate along multiple lineage pathways, including adipocytes, chondrocytes, myocytes, neurons and osteoblasts [81-84] as depicted in Figure 7.

The basic steps involved in isolation and culture of adipose derived ASCs are enumerated in Table 6. The human ASCs have a fibroblast like morphology and lack the intracellular oil typically seen in mature adipocytes. The adherent cells can then be cultured in medium that selectively promotes differentiation into mature adipocytes. Thus, after differentiation ASC can

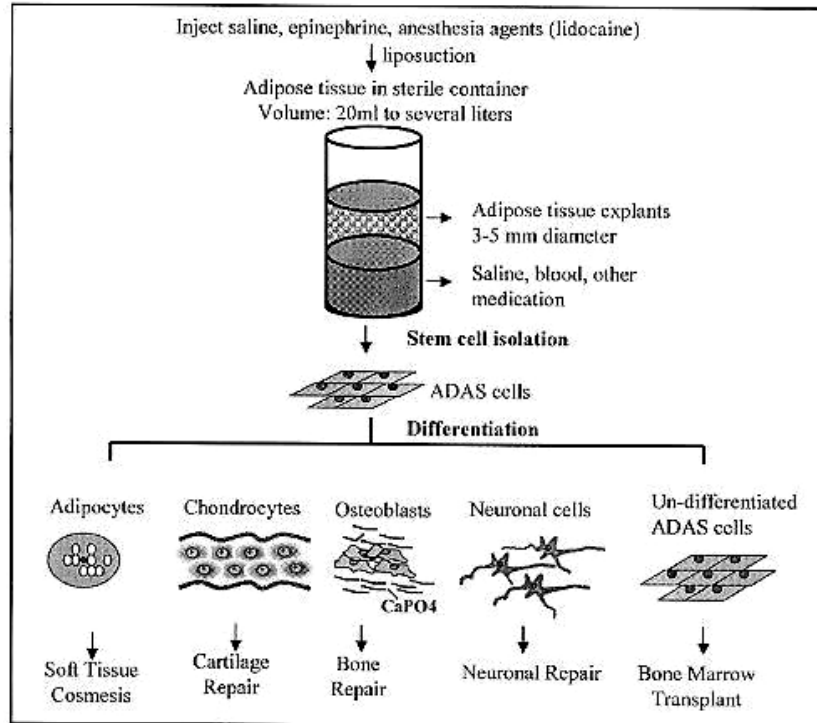


Figure 7 Adipose Derived Adult Stem cell expansion in culture along multiple lineage pathways, Burt *et al* [80].

Table 6 Isolation and Culture of adipose-derived adult stem cells, Burt *et al* [80].

Steps	Procedure
Isolation	Obtain liposuction waste material; Digest with type I collagenase Centrifuge; Isolate and wash stromal vascular pallet
Expansion	Plate on plastic wasve on presence of DMEM/F10 medium supplemented with 10% fetal hoving serum Feed after 1-3 days with medium supplemented with TGF β , EGF, bFGF
Harvest	At confluence, harvest cells for cryopreservation, immediate use of differentiate along lineage specific pathway
Differentiation	Adipogenic Factors – dexamethasone, indomethacin, isobutylmethylxanthine, insulin Osteogenic Factors – dexamethasone, 1, 2 dihydroxyvitamin D ₃ , ascorbate 2 phosphate, β glycerophosphate Chondrogenic Factors – dexamethasone, ascorbate, TGF β Myogenic Factors – 2-5% horse serum Neurogenic Factors – brain derived neurogenic factor, bFGF, EGF, antioxidant, valproic acid, forskolin, insulin

differentiate into chondrocytes for cartilage repair, osteoblasts for bone repair, neuronal cells for neuronal repair and undifferentiated ASCs can be used for bone marrow transplant.

Successful storage techniques for ASCs could revolutionize the fields of tissue engineering and regenerative medicine. The two competing strategies for long term storage of ASCs are freezing (cryopreservation) or desiccation (drying). An optimized desiccation procedure gives significant advantages over a standard cryopreservation protocol because the process of desiccation is simpler, quicker and has less toxic protectants that are added to the cells; storage conditions are less stringent and the logistics of transportation are simplified.

Successful drying and storage of ASCs using relatively simple methods would revolutionize the tissue engineering industry. To the best of our knowledge no work specifically related to drying storage of adipose derived ASCs has been reported. In the present study, the post-rehydration membrane integrity of various passages of ASCs dried in the presence of trehalose 50 mM and glycerol 384 mM has been examined. ASCs are dried using a convective drying stage at three different drying rates (slow, moderate and rapid) and stored for 48 hrs at three different storage conditions (ambient, plastic bags, and in vacuum). Upon rehydration the ASCs were incubated for 48 hrs in the stromal media before the ability of the ASCs to exclude fluorescent dyes was assessed. The results are analyzed to enhance the understanding of complex interactions between the drying medium, the drying rate, storage conditions and the passage of cells on the post-rehydration membrane integrity of ASCs.

2.2 Desiccation Protocols

2.2.1 Chemicals

All chemicals used in the entire process are procured from Sigma Aldrich Co, St. Louis, or mentioned otherwise. D-PBS with $MgCl_2$ and $CaCl_2$, liquid, sterile-filtered, cell culture tested is used to prepare the solution for incubating the ASC suspensions. D (+) Trehalose Dihydrate

from *S. cerevisiae* along with glycerol (Invitrogen Life technologies, Carlsbad, CA) was used as the protective agents during the drying of ASCs. Trypan Blue dye, sterile filtered prepared in 0.81% NaCl has been used for cell membrane integrity assay. Stromal Media used as one of the rehydrating agents of the ASCs is provided by Pennington Biomedical Centre, Baton Rouge, LA.

2.2.2 Isolation, Collection and Culture of Adult Stem Cells

All human protocols were reviewed and approved by the Pennington Biomedical Research Center Institutional Review Board. Subcutaneous adipose tissue liposuction aspirates were provided by plastic surgeons in Baton Rouge, LA. All procedures were conducted under aseptic conditions according to a modification of methods outlined in [85]. Tissue samples (100 to 200 ml) were washed 3-4 times in phosphate buffered saline (PBS) prewarmed to 37°C, suspended in PBS supplemented with 1% bovine serum albumin and 0.1% collagenase (Type I, Worthington Biochemicals, Lakewood, NJ), and digested with gentle rocking for 45-60 min at 37°C. The digests were centrifuged for 5 min at 1200 rpm (300× g) at room temperature, resuspended, and the centrifugation step repeated. The supernatant was aspirated and the pellet re-suspended in stromal medium (DMEM high glucose, 10% fetal bovine serum, 100 units penicillin/ml, 100 mcg streptomycin/ml, and 25 mcg amphotericin/ml). The cell suspension was plated at a density equivalent to 0.125 ml of liposuction tissue per cm² of surface area, using a 35 ml volume of stromal medium per T225 flask. Cells were cultured for 48 hrs in a 5% CO₂, humidified, 37°C incubator. At which time the adherent cells were rinsed once with prewarmed PBS and the cells fed with fresh stromal medium. The cells were fed with fresh stromal medium every 2-3 days until they reached approximately 75-80% confluence. The medium was then aspirated, the cells were rinsed with prewarmed PBS, and harvested by digestion with 0.05% trypsin solution (5-8 ml per T225 flask) for 3 to 5 min at 37°C. The cells were suspended in

stromal medium, centrifuged for 5 min at 1200 rpm (300× g), the pellet resuspended in a volume of 10 ml of stromal medium, and the cell count determined by trypan blue exclusion. These cells were identified as Passage 0 (P0). An aliquot of cells was reserved for freezing studies. The remaining cells were seeded in T225 flasks at a density of 5×10^3 cells per cm^2 . The cells were maintained in culture and passaged as described through successive Passages 1 to 4 (P1 to P4). Note that there is extensive data suggesting that these adherent cells exhibit multiple lineages when culture *in vitro* [86-94]. A recent study by Guilak *et al* [95] shows with the aid of histological and biochemical analyses that pools of human ASCs can exhibit multiple differentiated phenotypes under appropriate *in vitro* culture conditions (briefly, 52% of the ASC clones differentiated into two or more lineages; with more clones expressing osteoblasts, chondrocytes and neuron-like cells than adipocytes). Thus, there is clear evidence that the adherent cells cultured from stromal vascular fraction exhibit “stem cell” behavior, and are termed as human adipose derived adult stem cells (ASCs), in the present study.

2.2.3 Addition of Trehalose and Glycerol

For all drying experiments the ASC concentration was adjusted to be 1×10^6 cells/ml. Before drying, 1 ml stock solution of containing 768 mM glycerol and 100 mM trehalose was added to 1 ml of ASC suspension. Thus, the final concentration of in drying media was 50 mM trehalose and 384 mM glycerol. The ASCs were incubated at room temperature in the drying media for 30 min prior to conducting the convective drying experiments, described below.

2.2.4 Convective Drying Stage

A convective drying stage similar to the one described earlier by Bhowmick *et al* [64] was used in the present study to achieve controlled drying of P0 and P1 ASCs. Nitrogen gas (Doussan Inc., New Orleans, LA) from a pressurized cylinder was dried using an in line

desiccator drierite (W.A. Hammond Drierite & Co., Xenia, OH) and then exhausted through a Plexiglas chamber. The chamber was designed to hold three glass microslides, with each grooved microslide capable of holding a 10 μ l ASC suspension droplet. To ensure repeatable conditions, the entire flow path and the flow chamber were tightly sealed to prevent leakage. To ensure three different drying rates, the flow of nitrogen gas was controlled by adjusting the exhaust pressure using a pressure regulator (Doussan Inc.). Thus, three different drying rates were achieved, slow (with regulator pressure of 275 kPa), moderate (205 kPa) and rapid (140 kPa). After drying ASCs on the stage for 30 min, they were placed in a 6 well plate (Corning Plasticware Cell Culture, Sigma Aldrich, St Louis, MO) and stored at ambient temperature, or in plastic bags (Deni Magic Vac Bags, Keystone Manufacturing Company, Inc., Buffalo, NY) at ambient temperature or in a vacuum sealed bag (Deni Magic Vac™ Select, Keystone Manufacturing Company, Inc., Buffalo, NY). The samples were then stored for 48 hr. The schematic of the entire experimental set up is shown in Figure 8.

2.2.5 Assessment of Moisture Content in Dried Samples

Moisture measurements were made under different drying conditions. Gravimetric analysis was performed using an analytical balance (AE 163; Mettler, Columbus, OH). The % of moisture present is determined by Equation (1), as described elsewhere [64]. In Equation 1 the wet weight is the starting weight of the sample, the dry weight is the weight of the sample after the drying protocol has been completed and the baked weight is the weight after an equivalent sample has been heated overnight at 90°C for 24 h in an oven. The baked weight is assumed to be entirely free of moisture [46, 64].

2.2.6 Rehydration Protocol

After storing the ASC samples for 48 hr, they were rehydrated with 1 ml of D-PBS and 1 ml of stromal media. The mixture of the cell suspension and the media was allowed to

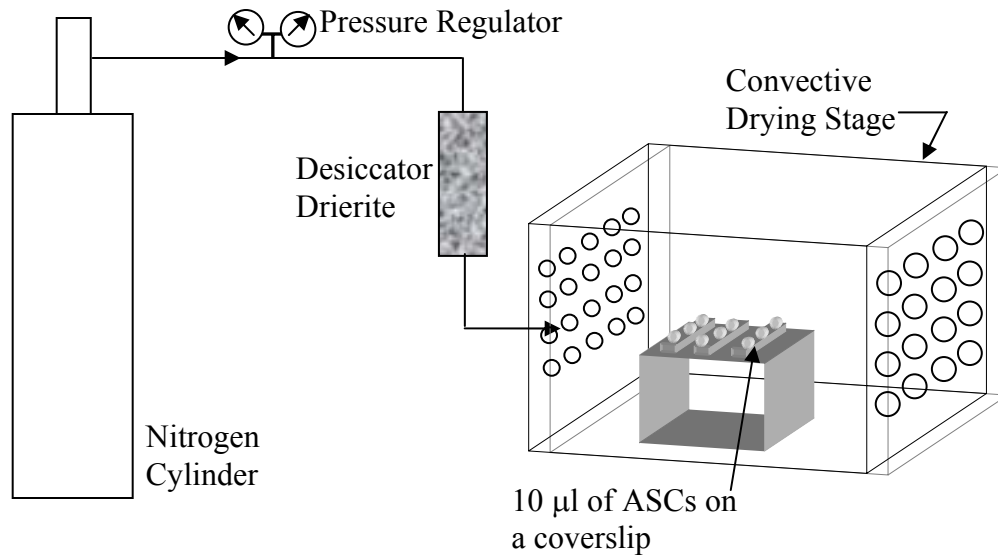


Figure 8 Schematic of the Convective Drying Stage (not to scale).

equilibrate briefly (~5 min), and then placed in an incubator (NAPCO-CO₂ incubator, Precision, VA) at 37°C, 5% CO₂ and 100% relative humidity (RH). After 48 hr, the cells were removed and their membrane integrity was assessed, as described below.

2.2.7 Cell Membrane Integrity Measurements

The membrane integrity assay was based on the ability of healthy cells with uncompromised cytoplasmic membrane integrity to exclude dyes such as trypan blue [96-98]. The cells were equilibrated with trypan blue solution for 15 min. After staining, the samples were placed on a microslide, cover slipped, and analyzed under a light microscope (Nikon Instruments Inc. Melville, NY, USA) at 10× magnification. The average cell survival, based on the ability of the rehydrated cell to exclude dyes, was defined as the ratio of the live cells to the total cells in the field of view.

2.3 Statistical Analysis

The data was analyzed using SAS 9.0. Experiments were repeated six times for each drying rate and storage condition. The data was analyzed by analysis of variance (ANOVA) using the SAS software. All data presented here represents a normal distribution. The results are expressed as mean value \pm Standard Error of Mean (SEM). Unless otherwise stated, all statistically significant differences in the data are reported with a probability of $P < 0.05$.

2.4 Results

2.4.1 Choice of Drying Media

Initially drying experiments were conducted to assess the relative impact of trehalose and glycerol on the post-rehydration integrity of ASCs and the recognition of a suitable media for conducting the intensive drying experiments. To this end, equal aliquots of either P0 or P1 ASCs were incubated for 30 min in either D-PBS alone or in D-PBS with 384 mM glycerol or in D-PBS with 384 mM glycerol and 50 mM trehalose. The ASCs were then dried using a convective drying stage for 30 min at a moderate drying rate, as described above. The % cell survival was estimated immediately (5 min) after the rehydration process using membrane excluded dyes. These preliminary experiments showed that the % P0 ASC survival in the presence of trehalose was significantly higher ($P < 0.01$) than in its absence ($72 \pm 3\%$ in the presence of trehalose and $56 \pm 5\%$ with glycerol and $26 \pm 8\%$ with D-PBS alone, Table 7) as shown in Figure 9. Similar results were obtained for P1 ASCs (data not shown). Then we proceeded to conduct exhaustive drying experiments with the drying media containing 50 mM trehalose with 384 mM glycerol. In summary, the experimental scheme in the present work comprises of drying two different passages of ASCs under three different convective drying conditions (slow, moderate or rapid) and three different storage conditions (ambient, plastic bags and in vacuum) using drying media

D-PBS with 50 mM trehalose, 384 mM glycerol as the drying media. Experiments with different media were repeated three times.

2.4.2 Convective Drying and Final Moisture Content

The convective drying setup described earlier was used to generate reproducible drying kinetics at different flow rates, as shown in Figure 8. Forced convective drying protocols were

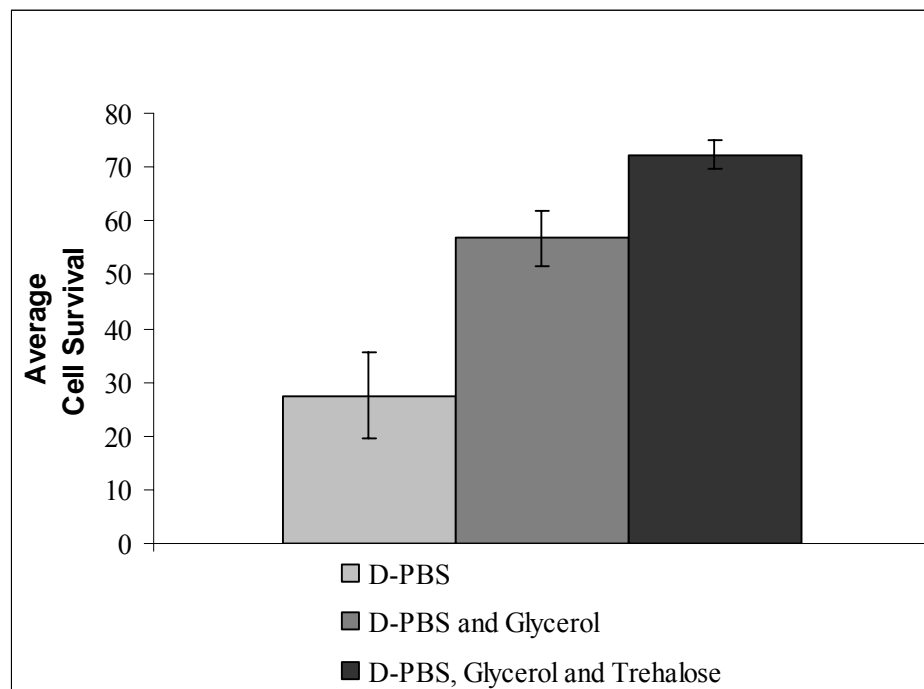


Figure 9 Effect of media on desiccation tolerance.

Table 7 Comparison of Average Cell Survival across Different Media.

Average Cell Survival in Different Media (equilibration time 30 min)		
	Mean	SEM
D-PBS	27.54	8.07
D-PBS +Glycerol	56.76	5.07
D-PBS + Glycerol + Trehalose	72.35	2.77

used at different pressures of dry nitrogen gas and are labeled as rapid, moderate and slow drying, respectively. Moisture content plot as presented in Figure 10 summarizes the weight fraction at different times of drying, with each experimental condition replicated six times for the drying media investigated. As observed in an earlier study [64], all three drying rates showed a similar trend of convective drying. The rapid drying curve is largely linear with ~9% of the initial weight being retained after 30 min of drying. As shown in Figure 10, the final weight fractions were ~21% and ~17% in slowly and moderately dried for DM1, respectively. The results also show that the final weight fraction was lowest in the rapidly dried samples and highest in the slowly dried samples. The moisture fraction was calculated for each sample using Equation (1), and the results are summarized in Figure 11.

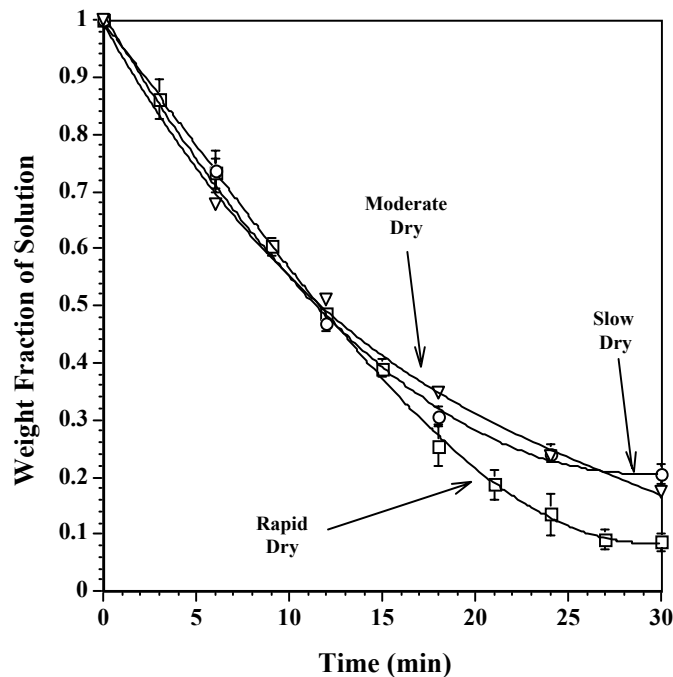


Figure 10 Plot of weight fraction (represented as the ratio of the final to the initial weight) vs. time (min) for three different drying rates, in media containing D-PBS with 50 mM trehalose and 384 mM glycerol.

Table 8 Data represented here are the means and standard errors of the means from 6 independent experiments for each passage using 50 mM Trehalose + 384 mM glycerol.

Cell Passage	Storage Conditions	Drying Conditions					
		Slow (275 kPa)		Moderate (205 kPa)		Rapid (140 kPa)	
		Mean	SEM	Mean	SEM	Mean	SEM
P0 ASC	Ambient	13.47	2.51	12.94	2.23	17.49	2.91
	Plastic Bags	9.34	1.83	15.11	2.97	13.48	2.11
	In Vacuum	37.35	2.64	18.58	2.45	22.80	3.33
P1 ASC	Ambient	3.65	0.61	2.72	0.7	2.30	0.56
	Plastic Bags	3.01	0.97	4.04	0.98	2.10	0.34
	In Vacuum	13.52	2.89	13.12	2.35	12.05	2.19

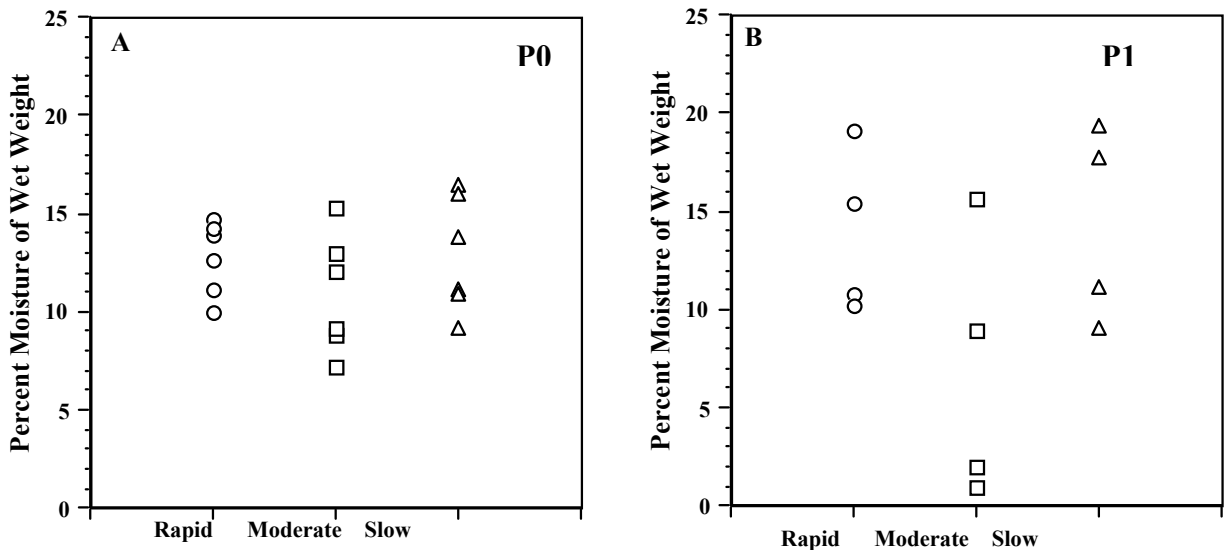


Figure 11 Dot plot of moisture content for P0 and P1 after various drying protocols: rapid (open circles), moderate (open squares) and slow (open triangles). All drying protocols carried out for 30min.

There are six separate sets of experiments for each of the three drying protocols for P0 and P1 ASCs, for a total of 36 experimental points. The resulting mean moisture percent for rapid-, moderate- and slow-drying protocols for P0 ASCs were 12.7 ± 1.9 %, 10.9 ± 3.0 %, and 12.9 ± 2.9 %, respectively. Similarly, the resulting mean moisture percent for rapid-, moderate- and slow-drying protocols for P1 ASCs in were 12.9 ± 4.1 %, 6.9 ± 3.2 %, and 13.9 ± 5.6 %, respectively.

2.4.3 Effect of Drying Rate and Storage Condition on ASC Membrane Integrity

A comparison of the post-rehydration membrane integrity is shown in Table 8 for P0 and P1 ASCs dried in the presence of 50 mM trehalose and 384 mM glycerol. For ease of analysis, a graphical representation of the data is shown in Figure 11 through Figure 13. In Figure 12, a comparison of the post-rehydration ASC membrane integrity is made for the three drying rates at each storage condition while in Figure 13, a comparison of the post-rehydration ASC membrane integrity is made for the three storage conditions at each drying rate. An examination of the data shows that: i) for P0 ASCs the optimal drying and storage conditions are slow drying and vacuum storage, respectively and ~37% of rehydrated ASCs are able to exclude dyes when slow dried and stored in vacuum; ii) for P0 ASCs dried either at a moderate or rapid drying rate, the % post-rehydration membrane integrity is independent of the storage condition and ranges from ~13% to 23%; iii) for P1 ASCs at a given storage condition, the % post-rehydration membrane integrity is independent of the drying rate, with the highest values (~12 to 14%) being obtained for vacuum stored samples; iv) for P1 ASCs, % post-rehydration membrane integrity of samples stored in either ambient environment or in plastic bags (~2 to 4%) are significantly smaller than vacuum stored samples (~12 to 14%); v) the maximum % of post-rehydration membrane integrity is significantly smaller for P1 ASCs (~14%) when compared with P0 ASCs (~37%).

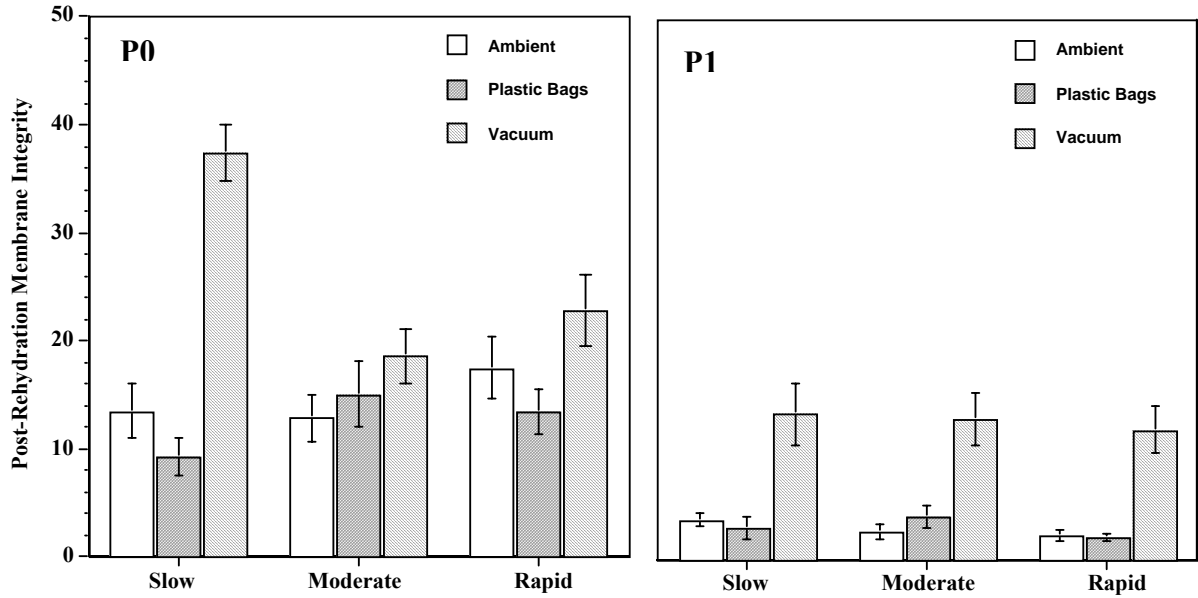


Figure 12 Comparison of the post rehydration membrane integrity across different flow rates.

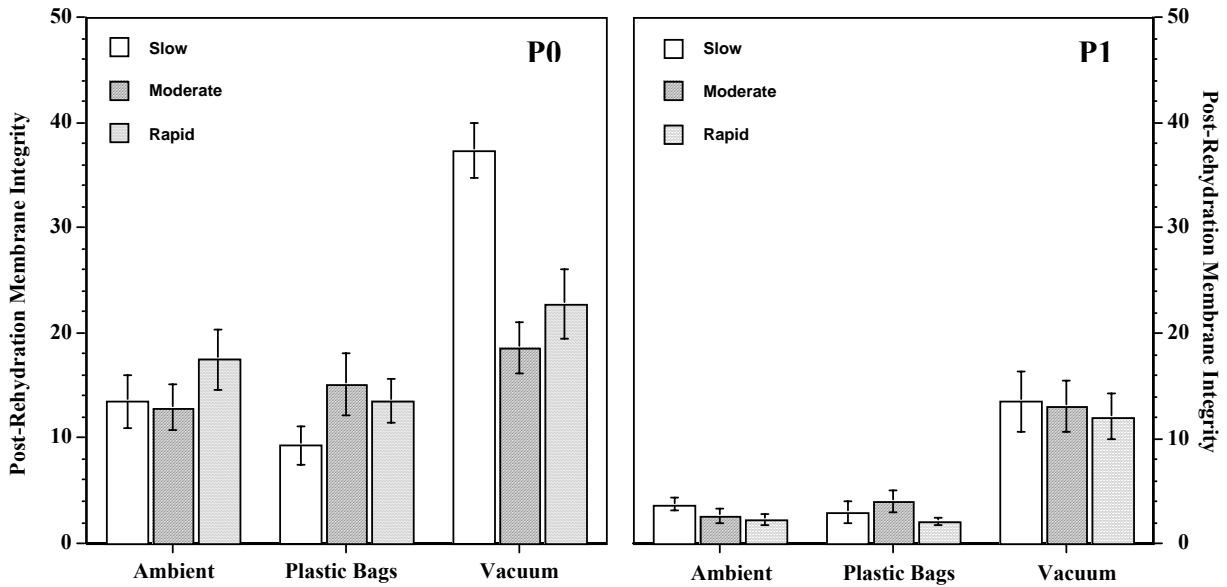


Figure 13 Post Rehydration Membrane integrity for P0 and P1 after drying and storage at i) at ambient temperature, ii) in plastic bags, iii) vacuum sealed bags at ambient temperature.

2.5 Discussion

2.5.1 Anhydrobiosis and Choice of Drying Media

Organisms have developed several novel and intriguing strategies for their survival when exposed to extreme cold, dryness, or heat, or the absence of oxygen [99]. This phenomena, involves a reversible suspension of the metabolism, an effective isolation from the environmental changes and the production of large amounts of saccharides [100, 101]. The mechanisms whereby sugars may stabilize living systems during freeze-thaw, heat-cooling, or dehydration-rehydration cycles remain a matter of debate. Among the sugars related with the mechanisms of anhydrobiosis, trehalose is one of the most effective protectants and has therefore been extensively studied [45, 100]. Consistent with these prior experiments, our experiments also showed that a significantly higher fraction of ASCs dried in the presence of trehalose retain their post-rehydration membrane integrity than its absence. Although, the exact reason for the protective action of trehalose is as yet unknown, it has been suggested that it reduces the mechanical stress imposed on the membrane during drying by maintaining the spacing between head groups and helps to keep the membrane in the fluid phase.

2.5.2 Intracellular Vs. Extracellular Trehalose

Previous studies on the desiccation tolerance of human cells revealed that trehalose could be expressed intracellularly with adenoviral vectors *otsA* and *otsB* genes [49]. Although, these genes are responsible for the conversion of uridine diphosphoglucose (UDP-Glucose) to trehalose, they exhibited significant cytotoxicity, particularly at multiplicities of infection [49]. Recently, Toner and colleagues reported the intracellular loading of trehalose by using a genetically engineered mutant of *Staphylococcus aureus* α -hemolysin to create pores in the cellular membrane [102] or by microinjecting trehalose [36] into oocytes. Although, de Castro and Tunnacliffe report that 80 mM intracellular trehalose is able to confer increased resistance to

the partial dehydration resulting from hypertonic stress in a genetically engineered mouse cell line, but does not enable survival of complete desiccation due to air drying. And finally, there is evidence to suggest that the presence of extracellular trehalose combined with permeating protectant (e.g. glycerol, dimethylsulfoxide) is beneficial for freezing preservation of fetal skin [103]. Prior evidence also suggests that incubation of adherent cells for 10 to 30 min with trehalose, in the absence of either a thermal or osmotic shock, does not result in a significant level of cell associated trehalose [50]. As we made no attempt to either induce intracellular trehalose or load trehalose into ASCs using pore forming techniques, our results only relate the effect of extracellular trehalose and a permeating protectant (glycerol) on the post-rehydration membrane integrity of ASCs. However, it is possible that ASCs might have “taken up” the extracellular trehalose by fluid-phase endocytosis or other mechanisms. This assertion is based on experimental evidence that suggest, trehalose is rapidly taken up by human platelets at 37°C, with loading efficiencies of 50% or greater via fluid-phase endocytosis or other mechanisms [47]. And finally, our method of adding glycerol and trehalose to ASC suspensions in a one step addition process might have caused osmotic shock to the ASCs and the consequent endogenous uptake or synthesis of osmolytes [50,104-106]. Typically these osmolytes are the disaccharide trehalose, the amino acid proline, and the trimethylammonium compound glycine betain [105, 106]. Future analysis by Fourier transform infrared spectroscopy are clearly needed to demonstrate if the membrane and protein components of trehalose-loaded ASCs pre-dehydration, post-drying and post-rehydration are similar to fresh ASCs.

2.5.3 Concentration of Trehalose and Optimal Drying Conditions

As shown in Table 5, a wide range of trehalose concentrations have been utilized during drying storage of mammalian cells. Puhlev *et al* [50] report that a concentration of 50 mM trehalose is optimal for Basinger cells and results in the highest degree of desiccation tolerance

with minimum cytotoxicity. Concentrations higher than 150 mM trehalose were found to induce obvious cytotoxicity in Basinger cells, probably due to prolonged exposure to hyperosmotic solutions [50]. However, Matsuo [53] reports that trehalose concentration of either 50 mM, or 100 mM or 200 mM provided desiccation tolerance to human corneal epithelial cells with no obvious cytotoxic effects at higher concentrations of trehalose. Ginnis *et al* [54] report successful desiccation preservation of mouse spermatozoa in the presence of 500 mM trehalose. Thus, in the present study, we chose to study the effect of the concentration of trehalose under 50 mM to provide desiccation tolerance to P0 and P1 ASCs.

To further assess the impact of drying ASCs in the presence of trehalose, we have also studied the effect of three different drying rates and three different storage conditions on the post-rehydration membrane integrity of P0 and P1 ASCs. For both P0 and P1 ASCs, slow drying and vacuum storage was found to be uniformly “optimal”. Our observations are consistent with earlier studies on human foreskin fibroblasts [49, 50] and human mesenchymal stem cells [52] which showed that slow drying coupled with vacuum storage has a dramatic positive effect on the retention of cellular viability of the desiccated cells. However, the actual mechanism involved in promoting the cellular viability in vacuum is as yet unknown. One possibility is that vacuum reduces the oxygen that is available to generate free radicals thereby minimizing the deleterious effects induced in the cells when they are stored at ambient temperature or in plastic bags. Another possibility is that the removal of air eliminates the meniscus effects that could damage the cells [49, 50].

In general, previous drying studies on mammalian cells suggest that slow drying and/or natural convection drying is optimal with ~5 to 10% residual moisture content [49-51, 53, 54, 107]. Our results are somewhat in agreement with this assertion, as slow drying resulted in a

higher fraction of rehydrated ASCs retaining their membrane integrity, especially for cells stored in vacuum. However, our experiments with natural convection drying (i.e., no flow rate of dry nitrogen gas) resulted in <1% cell survival (data not shown). Additionally, rapid drying seems to be somewhat better than either moderate or slow drying for P0 ASCs stored in the ambient environment and dried in media (DM1) containing 50mM trehalose and 384 mM glycerol. Although, the % final moisture content between the slowly and rapidly dried P0 ASCs in DM1 was not significantly different (Fig. 11; 12.7% vs. 12.9%). This observation, i.e. rapid drying being more efficacious than slow drying, is in agreement with earlier desiccation studies on embryonic axes of recalcitrant jackfruit seeds [108]. Intriguingly, the post-rehydration membrane integrity of P1 ASCs dried in the presence of DM1 was independent of the drying rate, i.e. for a given storage condition the rate of drying did not significantly affect the measured post-rehydration membrane integrity. However, the amount of final moisture content in P1 ASCs dried in DM1 ranged from 7 to 14%, suggesting that a reasonably wide range of final moisture content is optimal for P1 ASCs. Clearly, a more detailed study, possibly emulating a recent parametric study that described the effect of various freezing parameters on the post-freeze/thaw membrane integrity of ASCs [85], is needed to assess the relative impact of drying rate, the various components of the drying media, and the cell passage on ASC post-rehydration membrane integrity.

Finally, future experiments should be directed towards understanding the effect of rehydration kinetics on the membrane integrity of ASCs, a phenomenon that has been long known to influence the post-rehydration integrity of micro-organisms [109]. Recent evidence in *E. coli* suggests that there exists an optimal rehydration rate that permits maximum survival of preserved bacteria [110, 111]. This optimal rehydration is postulated to correspond to a rate that

is slow enough to allow the cell membrane to keep its integrity but rapid enough to prevent harmful perturbations of cell metabolism [110, 111]. Thus, it is quite possible that in future, determining the optimal magnitude and rate of rehydrating ASCs will lead to a further increase in their post-rehydration membrane integrity. Clearly, future studies are needed improve our understanding of drying storage of ASCs and will be conducted as time and resources permit.

2.6 Conclusion

In conclusion, we report here the effect of drying two different passages (P0 and P1) of adipose tissue derived adult stem cells (ASCs) in 50 mM trehalose with 384 mM glycerol at three different drying rates (rapid, moderate or slow) and three different storage conditions (ambient, in plastic bags and in vacuum). An important finding of this study was that significantly higher post-rehydration ASC membrane integrity is achieved when they are slow dried and stored in vacuum. Additionally, for a given combination of drying media, drying rate and storage condition, P1 ASCs had significantly lower post-rehydration membrane integrity than P0 ASCs. It is expected that the results presented here will lead to a better understanding of desiccation tolerance, and in the development of optimal drying storage protocols for ASCs.

CHAPTER 3. NUMERICAL INVESTIGATION OF THE PROPOSED SENSOR

3.1 Motivation

Desiccation offers the attractive possibility of storage of biological materials at ambient temperatures by simplifying the biopreservation protocols and logistics of transportation of preserved cells. In order to optimize and improve the drying techniques a thorough understanding of the loss of water (moisture) during drying of cell suspensions is essential. Hence, it is important to understand the extent to which a sample dries when subjected either to natural drying or forced convective drying process. The objective of the modeling conducted in this study is to design and optimize a sensor system that is capable of providing real time quantification of the weight loss during the drying process. The proposed novel sensor system uses ultrasonic technique and instrumentation. Recent studies have demonstrated that a class of sensors, known as resonant sensors, can be used for dynamically measuring a desired measurand [112-115]. Earlier studies have revealed that such dynamically varying physical parameters can be measured by making the desired measurand a function of the resonant frequency [116-118].

The present study is aimed at developing a technique to use the commercially available ultrasound transducers as a means to excite the designed resonant sensor during the drying of the cell suspension. It is expected that the shift of the resonant frequency of the sensor can be related to the change in mass during the drying process [71]. A one-dimensional (1-D) model is constructed to qualitatively understand the effect on the fundamental frequency of a vibrating beam during the drying process. The effect of various boundary conditions, absence and presence of mass and ultrasonic excitation on the fundamental frequency of the vibrating platform is evaluated.

It is important to understand the response of the sensor system to the external harmonic excitations caused by ultrasound. Harmonic excitations are a variety of applied forces that are proportional to trigonometric function $\sin(\omega t)$ or $\cos(\omega t)$ or a combination of both. These excitations are characterized by the fact that they repeat themselves. The frequency of each harmonic function is an integer multiple of the lowest frequency, which is known as the fundamental frequency. A great deal of information of the entire system under vibration can be obtained from a frequency spectrum, which involves a plot of the amplitude of vibration to the exciting (harmonic) frequency of vibration [119].

3.2 Mathematical Model

3.2.1 Assumptions

To represent a transversely vibrating model, a beam element is analyzed. Since the beam element has no rotating element, the rotational and the angular distortion effects due to shear on the beam are negligible and it is considered to be a Bernoulli-Euler Beam, rather than a Timoshenko beam. The six basic assumptions of an Euler-Bernoulli beam are as follow [119]:

1. The beam under consideration is long and slender which implies the following:
 - Length \gg Width
 - Length \gg Depth
 - The tensile and compressive stresses perpendicular to the beam are negligible than the tensile and compressive stress parallel to the beam.
2. The beam has a uniform cross section through out, i.e. $A(x) = A$.
3. The beam is loaded in the plane of symmetry. Euler-Bernoulli beam stipulates that the torsion inertia and shear deformation effects can be ignored. The product of the mass moment of inertia and angular acceleration is negligibly small.

4. During loading the deflection of the beam is very small. This simplifies the theory of elasticity in the elastic regime. This also accounts for no-buckling and no-plasticity condition of the material.
5. The material properties are isotropic and the beam considered is not soft.
6. The plane sections of the beam remain plane after loading.

The partial differential equation for bending vibration of the beam in the absence of an external force $F(x,t)$ is represented in Equation (5).

$$\frac{\partial^2}{\partial x^2} \left[E I(x) \frac{\partial^2 u}{\partial x^2} \right] + \rho A \frac{\partial^2 u(x,t)}{\partial t^2} = 0, \quad 0 < x < L \quad (5)$$

where, ρ is the density, $EI(x)$ is the flexural rigidity with E as the modulus of elasticity and $I(x)$ the cross sectional area moment of inertia about an axis normal to the x and y -axis passing through the centre of the cross-section, A is the area of cross section of the beam, $u(x,t)$ is the transverse displacement and $F(x,t)$ the transverse force per unit length. The effect of external forces $F(x,t)$ acting on a beam is represented in Figure 14. This specific boundary value problem can be derived using the Newtonian approach, by considering the differential element of length dx as shown in which Figure 14(b). $M(x,t)$ is the bending moment and $Q(x,t)$ is the shearing force acting on the element. Thus the partial differential equation for the bending vibration of a beam under $F(x,t)$ is represented as Equation (6) [119].

$$\frac{\partial^2}{\partial x^2} \left[E I(x) \frac{\partial^2 u(x,t)}{\partial x^2} \right] + \rho A \frac{\partial^2 u(x,t)}{\partial t^2} = F(x,t), \quad 0 < x < L \quad (6)$$

Thus, in order to solve the fourth order partial differential equation, two boundary conditions at each end have to be specified. The boundary conditions depend upon the mechanical

constructions at the end. A list of the most commonly used end construction and the corresponding boundary condition is given in Table 9.

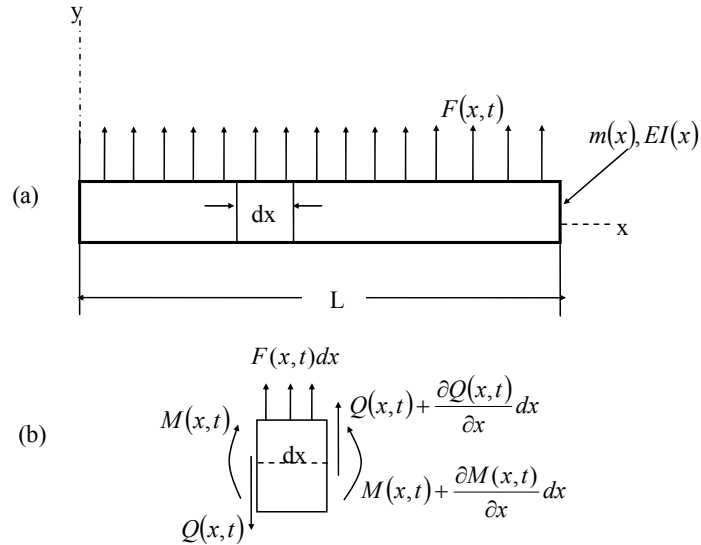


Figure 14 (a) Beam in bending vibration, (b) Free-body diagram for a beam element.

Table 9 Mechanical construction and the corresponding boundary condition.

End Construction	Boundary Condition	
Fixed End	Deflection = 0 $u(x,t) = 0$	Slope = 0 $\frac{\partial u(x,t)}{\partial x} = 0$
Pinned End	Displacement = 0 $u(x,t) = 0$	Moment = 0 $M(x,t) = EI(x) \frac{\partial^2 u(x,t)}{\partial x^2} = 0$
Free-End	Moment = 0 $M(x,t) = EI(x) \frac{\partial^2 u(x,t)}{\partial x^2} = 0$	Shear force = 0 $Q(x,t) = -\frac{\partial}{\partial x} \left[EI(x) \frac{\partial^2 u(x,t)}{\partial x^2} \right] = 0$

Table 10 Material properties of Titanium.

Property	Value
Modulus of Elasticity (E)	116×10^9 GPa
Density (ρ)	4500 kg/m ³
Poisson's Ratio (ν)	0.34

The first step in developing an analytical model for the resonating structure is to determine the material that is used in the construction of the vibrating beam. The material considered for the microplatform is Titanium, due to its unique combination of attributes such as biocompatibility, high durability in extreme environments, light weight and high strength. The material properties for titanium are presented in Table 10.

3.3 Design Constraints

The design constraints for developing the sensitive resonant sensor have been identified based on the actual experimental conditions. These design constraints are as follow:

1. The experimental work involves drying of 3 μ l -10 μ l of cell suspension, which typically occupies \sim 2 mm of space. Hence, the width of the beam has been fixed to be 2 mm.
2. The first natural frequency of the beam has to be of the order of 20 kHz or higher, so that it can be set into resonance by ultrasound.
3. Euler-Bernoulli beam assumptions should be satisfied.
4. The study of the effect on the resonant frequency for 90% water loss.

By optimizing the dimensions of the vibrating beam element the design criteria can be closely met. A detailed study of the resonating structure is carried out and all the steps involved in the modeling and analysis are outlined below. The first step in the present study was to determine the effect of the boundary condition on the fundamental frequency of vibration of the

microplatform. Ultrasonic techniques commonly use a water coupling between the transducer and sensor. Such an arrangement leads to the presence of air on one side and water on the other side of the sensor. Once the resonant frequency in vacuum is calculated the effect of media can be incorporated by using existing approaches [117].

3.4 Effect of Boundary Condition on the Fundamental Frequency

The effect of boundary conditions on the fundamental frequency of the beam is investigated as the first step in the analysis. The boundary conditions considered for the analysis are Fixed-Fixed Ends, Fixed-Pinned Ends, Fixed-Free Ends and Pinned-Pinned Ends. The effect of the boundary conditions on the fundamental frequency is shown in Figure 15. The plot for the variation of the fundamental frequency for different boundary conditions, length and thicknesses of the beam is obtained using the closed form solution obtained from the approach suggested by Blevins [120].

$$f_i = \frac{\lambda_i^2}{2\pi L^2} \left(\frac{EI}{m} \right)^{1/2} \quad i = 1, 2, 3... \quad (7)$$

where, λ_i is a dimensionless parameter, which is a function of the boundary conditions applied to the beam, L is the span of the beam, m is the mass per unit length of the beam (specified as $\rho \times A$, where A is the cross-section area and ρ is the density of the material of the beam). From Figure 15, it is observed that the ultrasonic frequency of vibration (20 kHz and above) of the beam can be achieved by utilizing the fixed-fixed boundary condition for the structure. This is because any additional constraint in restricting the motion of the vibrating beam implies higher stiffness and hence, greater frequency. The vibratory motion is most restricted in the fixed-fixed condition, therefore, the highest natural frequency is obtained in this configuration. The least fundamental frequency was observed for a pinned-pinned boundary condition. The presence of longitudinal

constraints will not affect the transverse vibrations of the beam because the longitudinal displacement is of second order ($\sim u^2$). As evident from Equation (7) the frequency of vibration depends on the non dimensional parameter λ . This parameter depends on the boundary conditions and its values are summarized in Table 11. The second step in modeling the

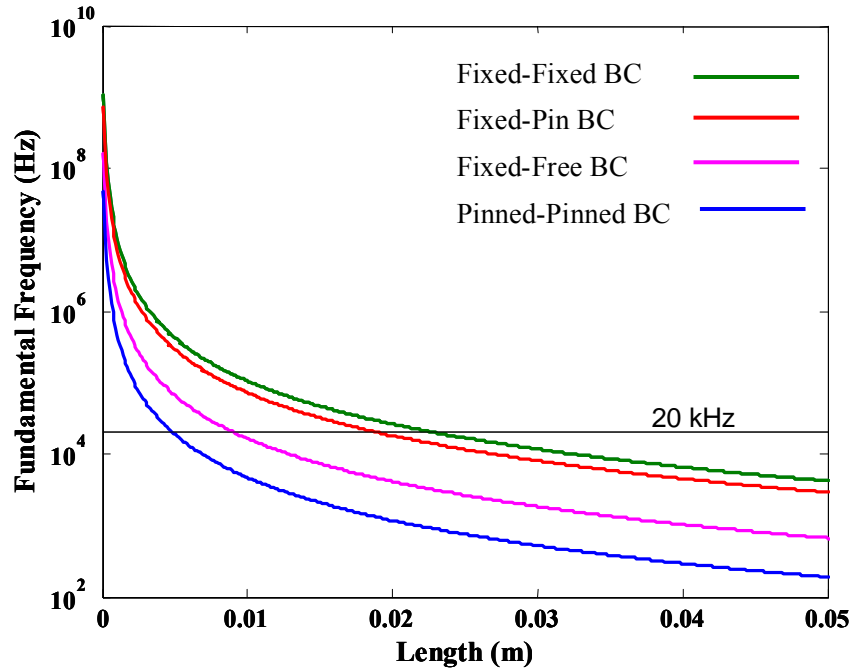
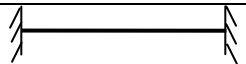
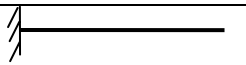
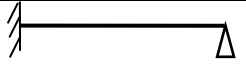


Figure 15 Effect of beam length on the fundamental frequency of the beam under four different boundary conditions.

Table 11 Value of non-dimensional parameter λ for different boundary conditions [120].

Description	Configuration of the Beam	Transcendental Equation for λ	Non Dimensional parameter λ_i (i=1)
	Fixed-Fixed	$\cos \lambda \cosh \lambda = 1$	4.7300
	Fixed-Free	$\cos \lambda \cosh \lambda + 1 = 0$	1.8751
	Fixed-Pinned	$\tan \lambda = \tanh \lambda$	3.9266

ultrasonic resonant sensor with a beam configuration and a fixed-fixed boundary condition is to optimize the dimensions.

3.5 Optimizing the Dimensions of the Vibrating Beam

The second step in modeling the ultrasonic resonant sensor with a beam configuration and a fixed-fixed boundary configuration is to optimize the beam dimensions. To design and optimize such a vibrating system the objective is to arrive at the dimension in the working range, which is in the ultrasonic range.

Since, the beam used is an Euler-Bernoulli beam it has to be long and slender, which implies that the following conditions should be satisfied.

$$\frac{Length}{Width} \gg 1 ; \frac{Length}{Depth} \gg 1 \quad (8)$$

From Equation (7), which represents the fundamental frequency of a beam, it can be inferred that the fundamental frequency is inversely proportional to the square of the length (L^2), independent of the width (w) and directly proportional to the thickness (h) as represented in Equation (9).

$$f = \frac{\lambda^2}{2\pi L^2} \left(\frac{Ewh^3}{12\rho A} \right)^{\frac{1}{2}} \quad (9)$$

$$f = \frac{\lambda^2}{2\pi L^2} \left(\frac{Ewh^3}{12\rho wh} \right)^{\frac{1}{2}} = \frac{\lambda^2 h}{2\pi L^2} \left(\frac{E}{12\rho} \right)^{\frac{1}{2}}$$

Thus, if the length is increased the frequency decreases by an order of ($1/L^2$) and the frequency increases as the thickness increases. The width of the sensor is fixed owing to the expected sample dimensions. Hence, depending on the width a suitable range for the length has to be selected to satisfy the Bernoulli constraint of slenderness of a beam. The optimization of length and thickness can be achieved by considering two cases of the vibrating sensor dimensions:

Case 1: When $\frac{Length}{Width}=1$ & $\frac{Length}{Thickness}=1$: If this equality is considered, for a width variation between 0.0015 m and 0.002 m the length variation will also be the same by the conditions of the equality and the Euler-Bernoulli formulation is violated. Varying the thickness in trends similar to the length also violates the basis of the beam formulation. Hence, Case 2 is considered for optimization of the dimensions of the beam.

Case 2: When $\frac{Length}{Width}$ lies between 1 and 25 and $\frac{Length}{Thickness}$ ratio lies between 1 and 12.5: The effect of variation of the length for a constant width of 0.002 m is observed in the analysis. For the length/width ratios between 1 and 25 the change in fundamental frequency is represented in Figure 16.

The effect of variation of thickness on the fundamental frequency of the beam is represented as two regimes, A and B in Figure 16. Regime A illustrates the effect on the first natural frequency when the thickness varies from 2×10^{-3} to 2.5×10^{-3} m. Regime B represents the variation of thickness from 10×10^{-3} to 50×10^{-3} m. From Figure 16 it can be observed that as the thickness is increased by a factor of 10, i.e., as we move from regime A to regime B, the fundamental frequency can be achieved in the ultrasonic range for longer lengths of the beam. This satisfies the slenderness ratio, length/width ratio, requirements posed by the Euler-Bernoulli equation for the beam. But, the increase in thickness, while going from regime A to regime B, makes the length and thickness to be of the same order, which causes a change in the configuration of the beam to a thin plate. Hence, the basic assumption of the Euler-Bernoulli beam is violated. The conditions satisfying or violating the Euler-Bernoulli assumptions are

schematically presented in Figure 17. On the other hand, if the thickness is restricted to regime A, then the ultrasonic range can be obtained for lengths between 0.02 m and 0.03 m, also shown in Figure 18, satisfying all Euler-Bernoulli assumptions. From Figure 18 it can be observed that if the length of the ultrasonic resonant sensor is increased from 0.028 m the natural frequency

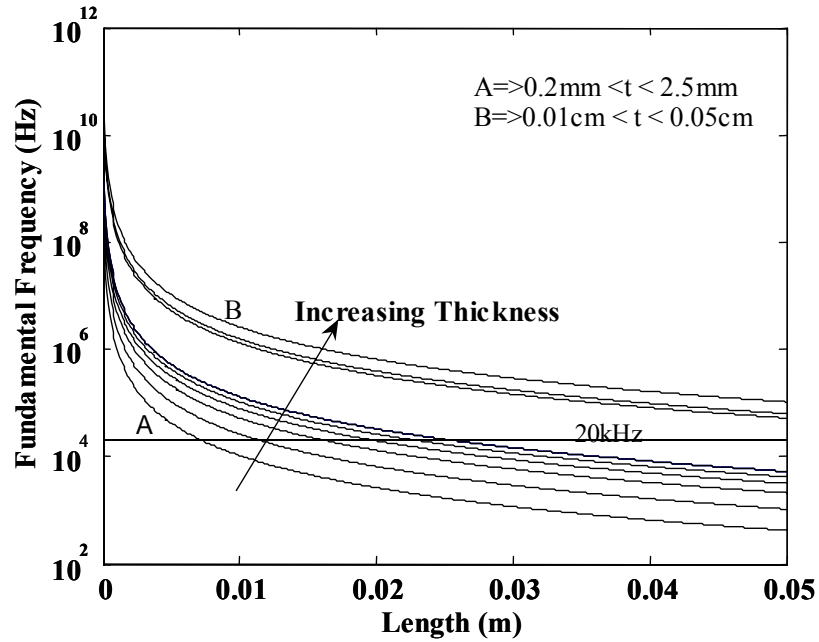


Figure 16 Variation of the fundamental frequency with length for different thickness.

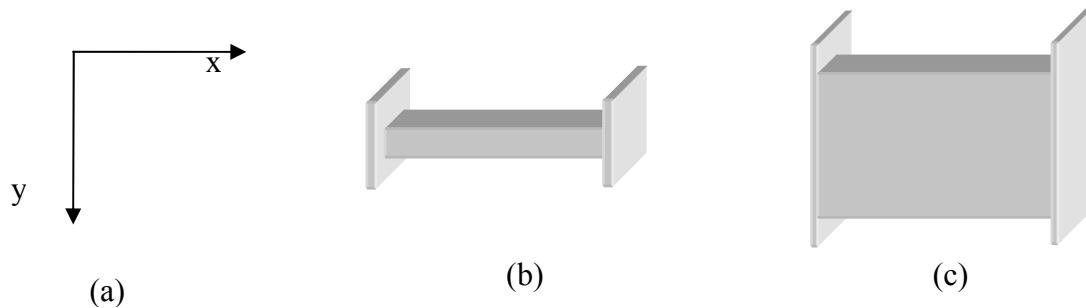


Figure 17 (a) Axis Representation (b) Euler-Bernoulli beam (c) Violation of Euler-Bernoulli beam assumption by increasing the thickness.

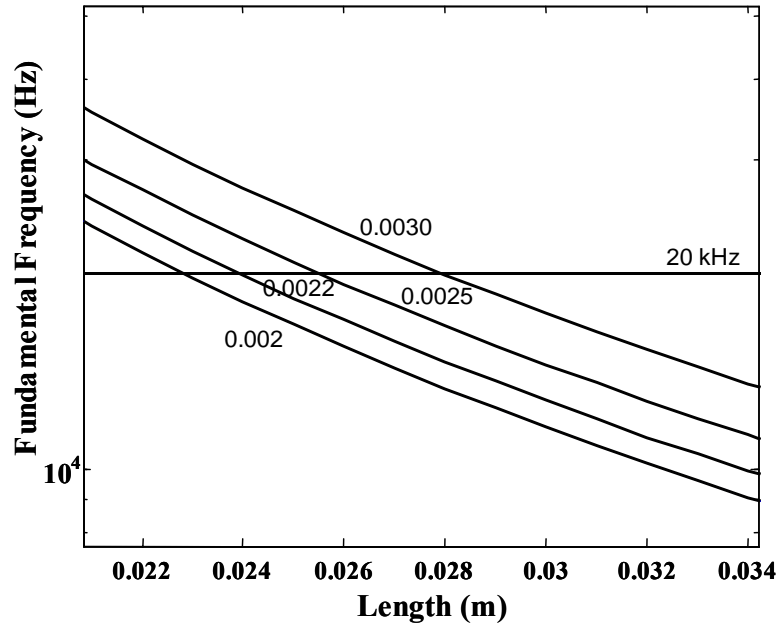


Figure 18 Working range of thickness and length for the ultrasonic sensor.

falls below 20 kHz for thickness between 20×10^{-4} and 30×10^{-4} m. Thus, by selecting the length as 0.025 m and thickness as 0.0025 m the fundamental frequency of 20.875 kHz can be achieved. By choosing these dimensions not only the fundamental frequency of the beam can be achieved in the ultrasonic region but also the Euler-Bernoulli assumptions for a beam can be satisfied.

3.6 Effect of Mass on the Ultrasonic Resonant Sensor

The previous steps involved optimizing the dimensions of the resonant sensor. Hence, the effect of change in the mass of the sensor on the fundamental frequency can now be calculated. The titanium based sensor of length 0.025 m, thickness 0.0025 m and width 0.002 m will resonate when excited with an ultrasonic frequency of 20.875 kHz. Now, the effect of loading of the cell suspension mass and reduction in mass due to drying on the fundamental frequency of the beam needs to be evaluated. To quantify the effect of mass on the first natural frequency, the *Transcendental Eigenvalue* formulation has been adopted.

3.6.1 Transcendental Eigenvalue Problem

Models of the vibrating system can be divided into two broad classes, lumped and continuous, depending upon the nature of the parameters that they are based on. In lumped systems, the components are discrete and the mass is assumed to be concentrated at individual points. The stiffness is accounted for by considering the masses to be connected by rigid massless rods. The masses and springs represent the system parameters in such models. To solve the lumped or discrete systems each mass is defined by an ordinary differential equation and the degree of freedom for the system is given by the number of masses in the system. Such systems can be solved by techniques from linear system theory.

Practical problems involving rods under axial deformation, shafts in torsion and beams in bending can be broken into an equivalent spring and mass system if their mass is neglected. When the mass of the system under vibration cannot be neglected then the system has to be treated as a continuous system or distributed parameter systems. The mass is defined in the form of mass per unit length and it represents the mass density for the beam element under vibration. By developing differential equations a continuous system can be solved using Transcendental Eigenvalue methodology. The method of formulation is described below.

In the absence of external excitations the partial differential equation for the transverse displacement $u(x, t)$ reduces to Equation (10).

$$-\frac{\partial^2}{\partial x^2} \left[EI(x) \frac{\partial^2 u(x, t)}{\partial x^2} \right] = m(x) \frac{\partial^2 u(x, t)}{\partial t^2}, 0 < x < L \quad (10)$$

The solution for Equation (10) must satisfy the boundary conditions at each end. During the synchronous motion of the beam, it exhibits a unique profile or shape, which does not change with time but only the amplitude of the profile changes. Mathematically, the solution for

Equation (10) can be expressed as a variable separable one, and the boundary value problem can be expressed as represented in Equation (11).

$$u(x, t) = U(x)F(t) \quad (11)$$

The *differential eigenvalue problem* for the vibrating beam consists of the *differential equation* shown in Equation (12), which involves determining the constant ω^2 such that Equation (12) admits nontrivial solution $U(x)$ that satisfies the boundary conditions

$$\frac{d^2}{dx^2} \left[EI(x) \frac{d^2 U(x, t)}{dx^2} \right] = \omega^2 m(x) U(x), \quad 0 < x < L \quad (12)$$

where ω is the frequency of the beam. Since, Equation (12) is a fourth order differential equation; there will be four constants of integration involved in the solution. The four constants of integration together with ω are the five unknowns that need to be determined in order to derive a solution for the differential equation. Hence, five conditions need to be specified in order to solve for five unknowns. Four boundary conditions can be specified pertaining to the type of end construction. Hence, using the four boundary conditions a *characteristic equation* is developed in which the constants are expressed in terms of each other. This characteristic equation is generally transcendental in nature, which has infinite number of roots known as eigenvalues. Corresponding to each of these roots there is an eigenfunction $U_r(x)$, which corresponds to the natural mode. Thus, for any type of distributed system the dynamics and stability can be formulated by transcendental eigenvalue problems, with transcendental eigen characteristic equations.

Both, lumped and continuous, systems possess natural modes, eigenvectors for discrete systems and eigenfunctions for distributed systems. The discrete system possesses finite number

of modes and the continuous system has an infinite number of modes. A characteristic equation is developed for continuous systems with infinite degrees of freedom and an algebraic eigenvalue problem is developed when analyzing the behavior of a multi-degree-of-freedom system as observed in discrete systems. In order to evaluate the effect of changing mass on the fundamental frequency of the beam the steps involved in solving a transcendental eigenvalue problem are followed, as described below.

3.6.2 Steps in Solving Transcendental Eigenvalue Problem Using Newton's Eigenvalue Iteration Method

By transcendental eigenvalue problem, we denote the problem of determining the non trivial solution ω and $z \neq 0$ of

$$A(\omega)z = 0 \quad (13)$$

Newton's Eigenvalue Iteration method can be used to derive the solution based on Yung's methodology [121, 122] by following the steps are listed as follows:

1. A matrix $B(\omega)$ is denoted as

$$B(\omega) = -\frac{dA(\omega)}{d\omega} \quad (14)$$

2. Using Taylor's series the expansion of $A(\omega)$ about $\omega(0)$ is obtained as

$$A(\omega^{(0)} + \varepsilon) = A(\omega^{(0)}) - \varepsilon B(\omega^{(0)}) + o(\varepsilon^2) \quad (15)$$

where $o(\varepsilon^2)$ includes second and higher order terms of ε .

3. Ignoring the second-and higher order terms of ε gives

$$\det[A(\omega^{(0)} + \varepsilon)] = \det[A(\omega^{(0)}) - \varepsilon B(\omega^{(0)})] \quad (16)$$

4. In the neighborhood of the eigenvalue ω represented in Equation (14)

$$\omega = (\omega^{(0)} + \varepsilon) \quad (17)$$

Thus,

$$\det[A(\omega^{(0)}) - \varepsilon B(\omega^{(0)})] = 0 \quad (18)$$

5. Hence, from Equation (14)

$$[A(\omega^{(0)}) - \varepsilon B(\omega^{(0)})]z = 0 \quad (19)$$

6. From Equation (18) it can be inferred that ε can be determined by the solution of eigenvalue problem. By starting with an initial guess we may determine a new value of ω in the i^{th} iteration as

$$\omega^{(i)} = \omega^{(i-1)} + \varepsilon^{(i)} \quad (20)$$

where $\varepsilon^{(i)}$ is the eigenvalue of

$$[A(\omega^{(i-1)}) - \lambda B(\omega^{(i-1)})]z^{(i-1)} = 0 \quad (21)$$

For a given $\omega^{(i-1)}$, there are generally n eigenvalues λ_i , $i = 1, 2, \dots, n$, where n is the dimension of the system. When the iterative process converges after m iterations the eigen vectors can also be determined.

7. For the case when $n = 1$, the $f(\omega) = A(\omega)$, and Equation (19) reduces to

$$\lambda = -\frac{f(\omega^{(i-1)})}{f'(\omega^{(i-1)})} \quad (22)$$

Thus, the new value of ω can be determined.

3.7 Effect of Mass on the Frequency - Using Transcendental Eigenvalue Formulation

The methodology to solve the current beam problem is represented in Figure 19, where the beam is split into two beams. The differential equation for the two beams having a uniform cross section is represented by Equation (23).

$$\begin{aligned} E I \left[\frac{\partial^4 u_A}{\partial x^4} \right] + \rho A \frac{\partial^2 u_A(x,t)}{\partial t^2} &= 0, \quad 0 < x < a \\ E I \left[\frac{\partial^4 u_B}{\partial x^4} \right] + \rho A \frac{\partial^2 u_B(x,t)}{\partial t^2} &= 0, \quad a < x < b \end{aligned} \quad (23)$$

Assuming that each point on the beam vibrates harmonically, then a solution $u(x,t) = V(x)\sin \omega t$ is tried. The non-dimensional differential equation for the given eigenvalue problem is presented by Equation (24) which has been described by Low and Rao [123, 124].

$$\frac{d^4 V_i}{dx^4} - \lambda^4 V_i = 0; \quad i = 1, 2 \quad \text{where} \quad \lambda^4 = \frac{\rho A L^4 \omega^2}{E I} \quad (24)$$

To solve such a boundary value problem, four boundary conditions given in Table 12 are required. Similarly to account for the centrally loaded mass, four continuity conditions are specified which are presented in Table 13.

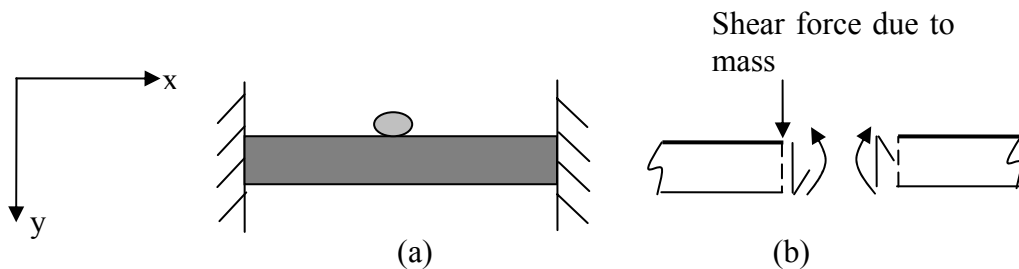


Figure 19 (a) Schematic of mass on a beam (solving using transcendental eigenvalue problem) (b) free body diagram of the split beam.

Table 12 Boundary Conditions for Beam 1 and 2 at the fixed ends.

Beam 1	Beam 2
$V_1(x = L) = 0$ <i>No Displacement</i>	$V_2(x = L) = 0$ <i>No Displacement</i>
$\frac{\partial V_1}{\partial x}(x = 0) = 0$ <i>No Slope</i>	$\frac{\partial V_2}{\partial x}(x = L) = 0$ <i>No Slope</i>

Table 13 Four Continuity Conditions where the mass is loaded to maintain continuity.

Condition	Mathematical Expression
Displacements are equal	$V_1(\alpha, t) = V_2(\alpha, t)$
Slopes are equal	$\frac{\partial V_1}{\partial x}(\alpha, t) = \frac{\partial V_2}{\partial x}(\alpha, t)$
Moments are equal	$\frac{\partial^2 V_1}{\partial x^2}(\alpha, t) = \frac{\partial^2 V_2}{\partial x^2}(\alpha, t)$
Shear Forces are equal.	$V_1''''(\alpha) + \beta\lambda^4 V_1(\alpha) - V_2''''(\alpha) = 0$

In Table 13 primes denote the differentiation with respect to the spatial variable x , the mass ratio

is defined as $\beta = \frac{M}{\rho AL}$ where M is the mass of cell suspension, and the dimensionless position

parameter is defined as $\alpha = \frac{a}{L}$. The general solution to Equation (24) is given in Equation (25)

$$\begin{aligned} V_1 &= D_1 \sin \lambda x + D_2 \cos \lambda x + D_3 \sinh \lambda x + D_4 \cosh \lambda x \\ V_2 &= D_5 \sin \lambda x + D_6 \cos \lambda x + D_7 \sinh \lambda x + D_8 \cosh \lambda x \end{aligned} \quad (25)$$

To solve Equation 25 for the unknowns, which correspond to 8 constant coefficients and the unknown λ , four classical boundary and four continuity conditions specified are used to develop an 8×8 matrix. This yields a classical transcendental eigenvalue problem of the form given in Equation

$$\mathbf{A}(\lambda_i, \alpha_i, \beta_i) \mathbf{z} = 0, \quad (26)$$

where $A(\lambda_i)$ is the matrix that consists of the co-efficient of the eigen vector and depends upon the boundary and matching conditions, z is the matrix that consists of the constant coefficients. Using the transcendental eigenvalue problem the value of λ_i is found that makes the matrix $A(\lambda_i)$ singular as developed by Singh *et al* [122]. The matrices that are developed are shown in the Appendix. For an unloaded beam the eigenvalue corresponds to the first eigenvalue of the fixed-fixed structure, the value being equal to 4.7300.

In the experimental part of the study, as presented in Chapter 2, ASCs were dried under three flow rates of nitrogen, i.e., 140 kPa, 205 kPa and 275 kPa for 30 min. The protocol involved measuring the weights of the cell suspension before and after drying. Hence, to evaluate the drying process, the effect on the frequency of the vibrating beam due to the changing mass is evaluated. The averages of the initial wet and final dried weight obtained from the experimental study are presented in Table 14. The calculated fundamental frequencies of the beam loaded with various wet and dried weights are presented in Table 15.

When a long slender beam is loaded with mass a reduction in the first natural frequency is observed. The variation of the frequency along the length of the beam is presented in Figure 20. Since the ends of the beam are fixed, the deflections at $x = 0$ and $x = L$ are found to be minimum. On the contrary, it has been observed that the effect on the natural frequency is highest when the mass is placed at the centre.

The effect of the change in mass on the eigenvalues is also observed. As the mass reduces due to drying of the cell suspension the fundamental frequency, which is related to the eigenvalue, increases. Figure 21 represent the increase in this value when there is reduction in mass by 10% to 90%. A relationship between the change in % change in eigenvalue and % change in mass is shown in Figure 22.

Table 14 Weights of samples before and after drying.

Rate of Drying	Wet Weight (g)	Dry Weight (g)	Wet Weight normalized w.r.t to weight of the beam	Dry Weight normalized w.r.t to weight of the beam
Rapid (140 kPa)	0.009917	0.0014	0.01763	0.002489
Slow (275 kPa)	0.01035	0.0015	0.0184	0.002667

Table 15 Fundamental Frequency Due to the presence of weight on the vibrating beam.

Rate of Drying	Wet Weight normalized w.r.t to weight of the beam	Fundamental Frequency (kHz)	Dry Weight normalized w.r.t to weight of the beam	Fundamental Frequency (kHz)
None	-	20.875	-	20.875
Rapid (140 kPa)	0.01763	20.425	0.002489	20.814
Slow (275 kPa)	0.0184	20.406	0.002667	20.804

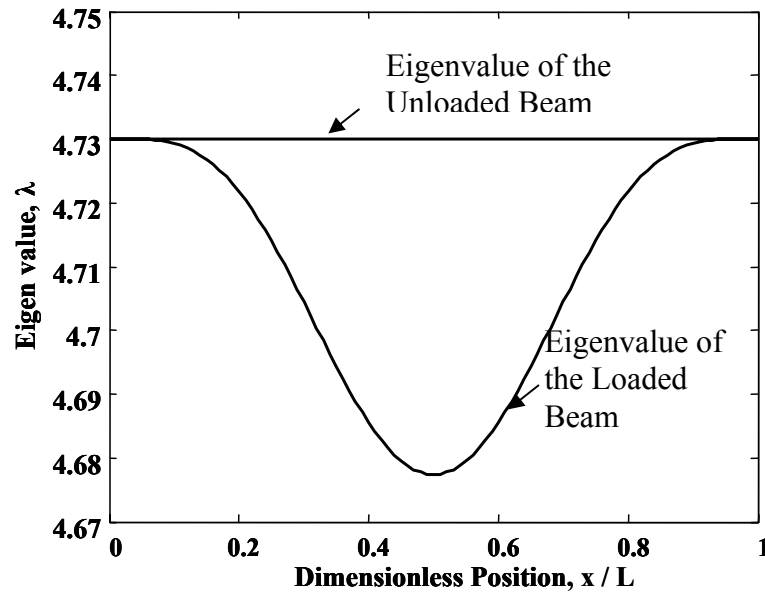


Figure 20 Effect on the eigenvalue due to the presence of mass

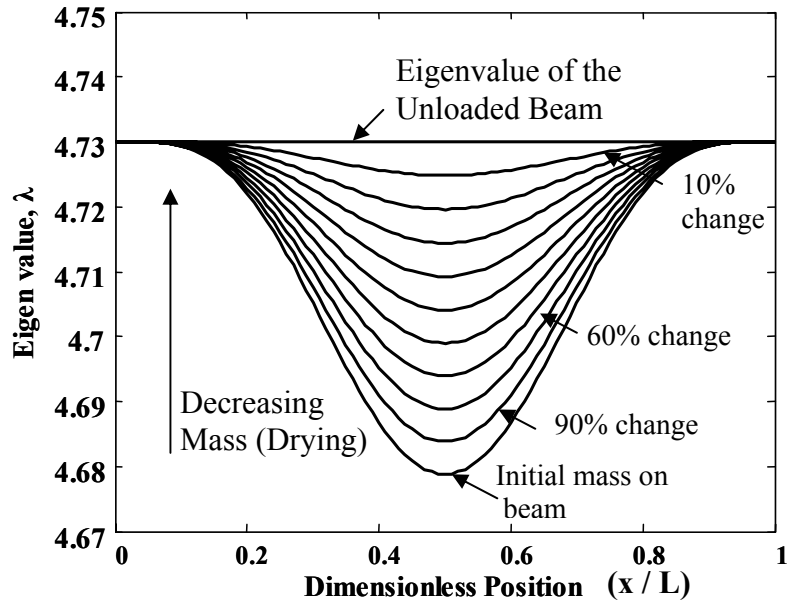


Figure 21 Effect on fundamental frequency due to change in mass.

From Figure 22 it can be observed that a linear relationship exists between the % change in eigenvalue to % change in mass. At the instant when the drying process is initiated by the convective flow of dry nitrogen there is no change in mass, hence, no change in frequency. As the mass starts decreasing there is a considerable effect on the fundamental frequency. The effects of an increase in the elastic restoring force and mass have been previously studied [125]. For each normal-mode vibration, the energy of the system can be described by Equation (27).

$$K(t) + V(t) = E = \text{const.} \quad (27)$$

If the average kinetic and potential energies are represented by $\overline{K(t)}$ and $\overline{V(t)}$, then the relation between them and the total energy can be represented by Equation (28).

$$\overline{K(t)} = \overline{V(t)} = \frac{1}{2} E \quad (28)$$

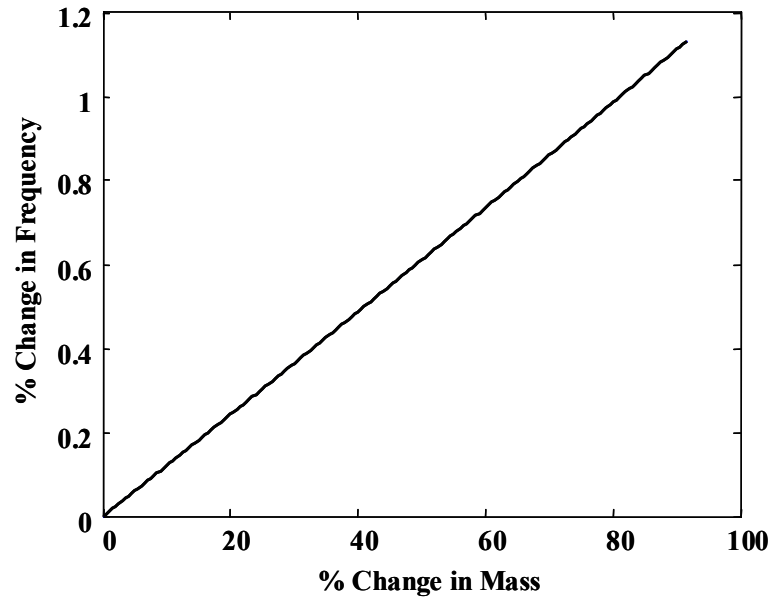


Figure 22 Effect of change in frequency with change in mass.

The values of $\overline{K(t)}$ and $\overline{V(t)}$ are related to the amplitude A and frequency ω in the manner represented in Equation (29).

$$\begin{aligned}\overline{K(t)} &= \beta\omega^2 A^2 \\ \overline{V(t)} &= \alpha A^2\end{aligned}\quad (29)$$

where the constants α and β are independent of the value of the amplitude A . The value of α depends on the elastic properties and β depends on the inertial properties of the vibratory system under consideration. Considering Equation (28), α and β can be related by Equation (30).

$$\omega = \left(\frac{\alpha}{\beta}\right)^{1/2}\quad (30)$$

The effect of mass and various boundary conditions can be considered as certain “perturbations” in the equation of motion in the normal-mode of vibration. By constraining the

motion of the beam by clamping, there is a change in the elastic restoring force. For such an elastic perturbation there is no change in the inertial component to the system. For the additional elastic restoring force there is an increment in α , which accounts for the average potential energy, by $\delta\alpha$, with minimal change in β . Let $\delta\bar{V}$ be the increase in the potential energy, then from Equation (31) the relation between the average potential energy and α can be established [125].

$$\frac{\delta\alpha}{\alpha} = \frac{\delta\bar{V}}{\bar{V}} \quad (31)$$

The value of α changes with the changes in the boundary condition and without any change in β there is an increase in the frequency as established by Equation (32).

$$\frac{\delta\omega}{\omega} = \frac{1}{2} \frac{\delta\alpha}{\alpha} \quad (32)$$

Thus, for a given value of the amplitude A an increase in α implies an increase in \bar{V} , equal to \bar{K} from Equation (28), which results in an increase in the frequency. The reason for decrease in the frequency due to mass loading is due to the increase in β (the factor that relates to the inertial mass of the system). This is because a fractional increase in β equals a fractional increase in average kinetic energy as represented in Equation (33).and Equation (34).

$$\frac{\delta\beta}{\beta} = \frac{\delta\bar{K}}{\bar{K}} \quad (33)$$

$$\frac{\delta\omega}{\omega} = -\frac{1}{2} \frac{\delta\beta}{\beta} \quad (34)$$

The increase in β by $\delta\beta$ with a negligible change in α necessitates a decrease in the frequency which is related to the effect of mass loading.

3.8 Frequency Response of the Beam under Ultrasonic Excitation

The response to harmonic excitations is a steady state response and is best treated in the frequency domain. The frequency spectrum is termed as frequency response plots. Frequency-response plots are two companion diagrams that represent how the amplitude and phase angle of the response vary as the excitation frequency changes.

The sensor system considered here is a conservative system. The concept of resonance can be illustrated using a single degree of freedom (SDOF) system. The equation of motion of a SDOF system is given in Equation (35), where $F(t)$ is the external harmonic force.

$$m \ddot{x} + kx(t) = F(t) \quad (35)$$

If the external harmonic force is given as $f(t) = A \sin \omega t$, then equation (35) can be written as Equation (36).

$$\ddot{x} + \omega_n^2 x(t) = \omega_n^2 A \sin \omega t \quad (36)$$

where ω_n is the natural frequency of vibration. It has been observed that harmonic forces are steady-state excitations, for which time plays a secondary role due to which the response is also steady. Hence, when the frequency of the external vibrating force equals the natural frequency the system goes into resonance.

3.9 Procedure for Analyzing Frequency Response of Beam

The beam is divided into two parts and the solution matrix is formulated with four boundary and four matching conditions.

$$\frac{\partial^2}{\partial x^2} \left[E I(x) \frac{\partial^2 u(x,t)}{\partial x^2} \right] + \rho A \frac{\partial^2 u(x,t)}{\partial t^2} = \sin \omega t, \quad 0 < x < L \quad (37)$$

The boundary conditions are as specified in Table 12. The modified matching conditions including the effect of the harmonic ultrasonic excitation are given in Table 16. Here, it is assumed that ultrasound travels in straight path rather than in waves and excites the beam exactly at the point where the mass is placed, which is similar to the case in focused probe transducers. The frequency response of the unloaded beam is shown in Figure 23. The effect of the presence of mass on the resonant frequency of the beam excited by ultrasound is observed by a shift in the response plot shown in Figure 24. From the figure it is observed that the response shifts to the left which indicates that the frequency decreases due to the presence of mass on the beam.

The effect of 10%, 20%, up to 90% change in mass are represented in Figure 25, Figure 26 and Figure 27, respectively, by a shift in the resonant frequency. Hence, a shift between the changes in mass is established with the change in the resonant frequency of the structure.

From the results a relationship between the shift in resonant frequency caused due to the change in mass is established. % change in the resonant frequency w.r.t to the % change in mass shows a linear trend as represented in Figure 28, which is indicative of the fact that if the change in resonant frequency is known the change in the mass can be determined from the graph.

Table 16 Matching conditions including the effect of ultrasound

Condition	Mathematical Expression
Displacements are equal	$V_1(\alpha, t) = V_2(\alpha, t)$
Slopes are equal	$\frac{\partial V_1}{\partial x}(\alpha, t) = \frac{\partial V_2}{\partial x}(\alpha, t)$
Moments are equal	$\frac{\partial^2 V_1}{\partial x^2}(\alpha, t) = \frac{\partial^2 V_2}{\partial x^2}(\alpha, t)$
Shear Force accounting for ultrasonic excitation	$V_1'''(\alpha) + \beta\lambda^4 V_1(\alpha) - V_2'''(\alpha) = \sin \omega t$

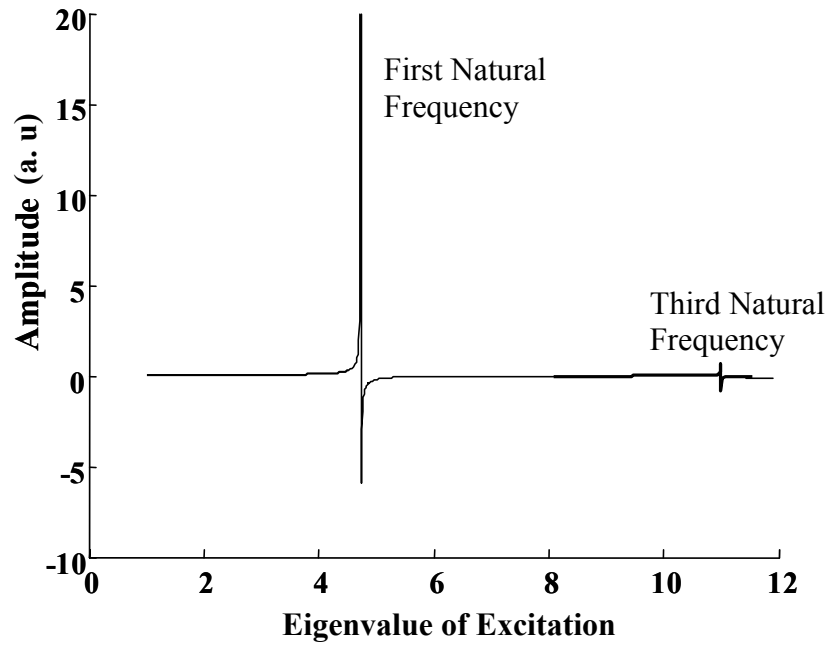


Figure 23 Frequency response of an unloaded beam.

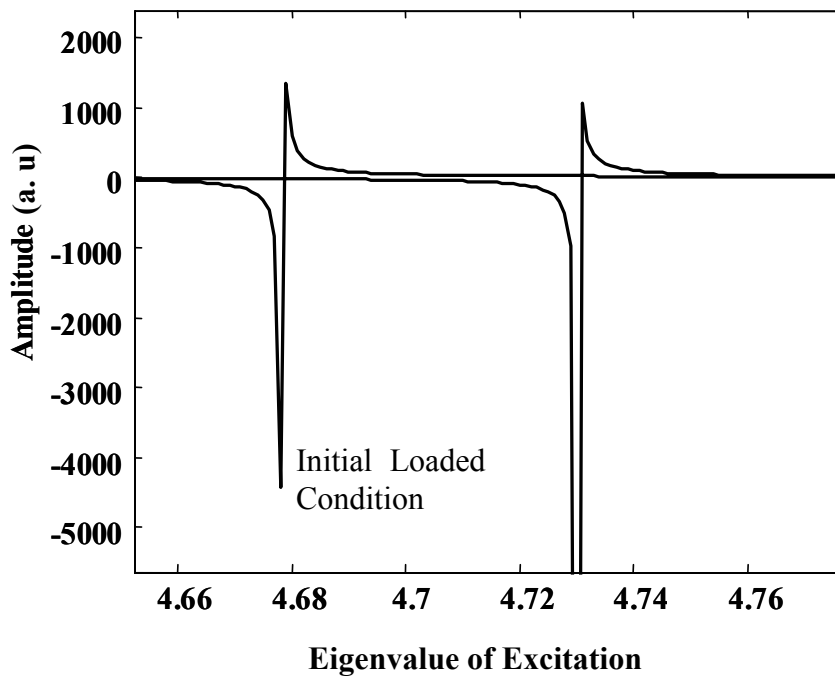


Figure 24 Shift in the resonant frequency is related to the change in mass.

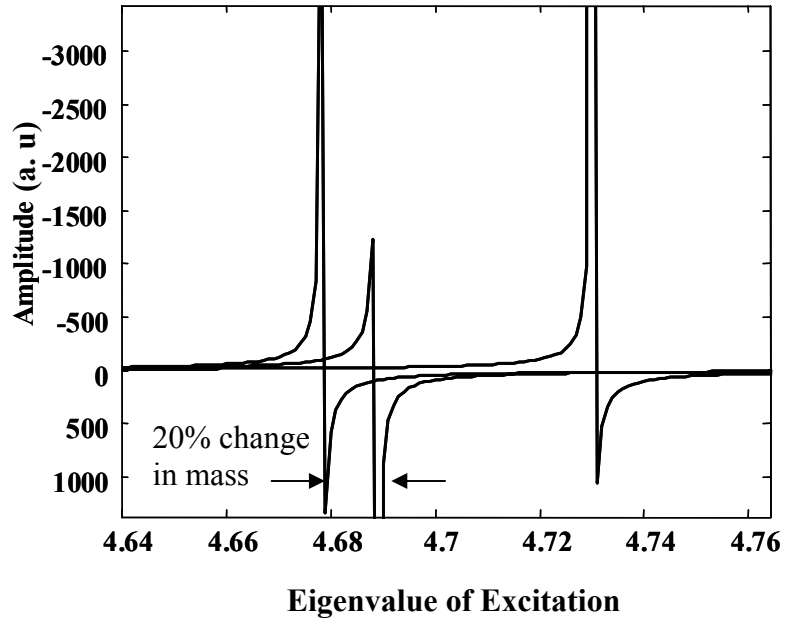


Figure 25 Shift in resonant frequency due to 20% change in mass.

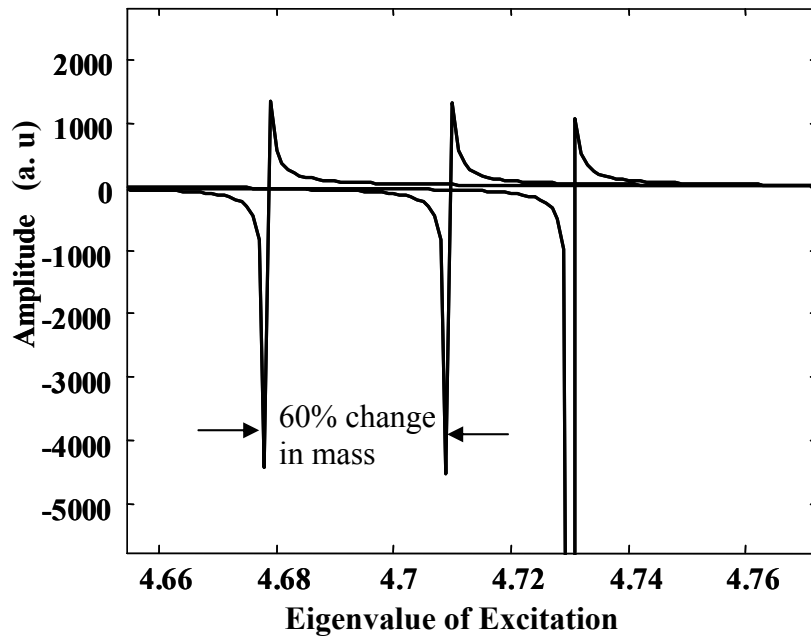


Figure 26 Shift in resonant frequency of the beam due to 60% change in mass.

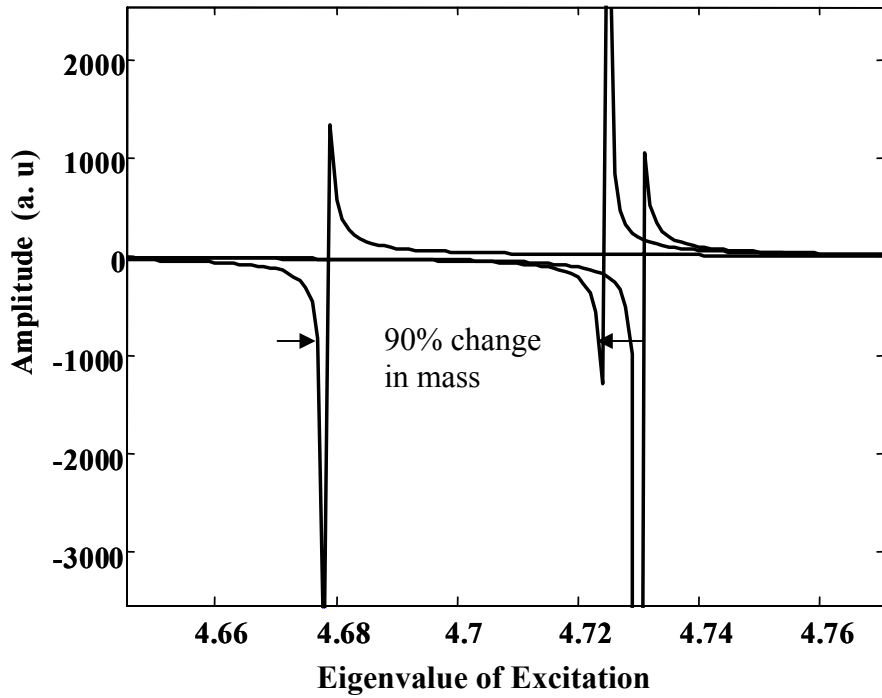


Figure 27 Shift in resonant frequency of the beam due to 90% change in mass.

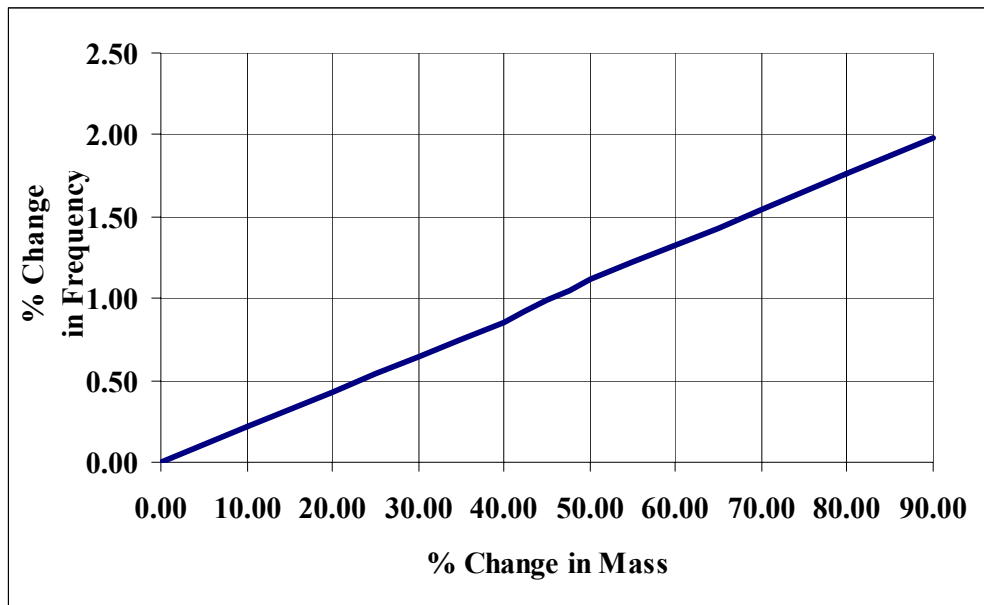


Figure 28 A linear relationship between the % change in the resonant frequency to the % change in mass brought about by drying.

Once the first natural frequency of beam is obtained the effect of the media can be incorporated using Equation (38) [117],

$$f = \frac{f_{vac}}{\sqrt{1 + \left(\frac{\rho_w}{\rho} + \frac{\rho_a}{\rho} \right) \left(\frac{b}{h} \right) \left(\frac{g}{2} \right) (0.6904)^2}} \quad (38)$$

where ρ , ρ_w and ρ_a are the densities of material of the beam, water and air, respectively .

3.10 Extension of the Beam Model to a Plate Model

Plates are straight, plane (flat, noncurved) surface structures whose thickness is small compared to other dimensions. Plates have free, simply supported and fixed boundary conditions, including elastic supports, elastic restraints or point supports. The static or dynamic loads carried by plates are predominantly perpendicular to the plate surface. The load-carrying action of plates resembles to, a certain extent, that of beams. Various types of plates can be divided into the following major categories based on their structural action:

1. Stiff Plates: thin plates with flexural rigidity, carrying loads two dimensionality, mostly by internal (bending or torsional) moments and by transverse shears, generally in a manner similar to beams.
2. Membranes: thin plates without flexural rigidity; carry the lateral loads by axial and central shear forces. The load carrying action can be approximated by a network of stressed cables, since, their moment resistance is of a negligible order of magnitude because of their extreme thinness.
3. Flexible plates: represent a combination of stiff plates and membranes and carry external loads by the combined action of internal moments, transverse and central shear forces,

and axial forces. Such plates are widely used by the aerospace industry because of their favorable weight-to-load ratio.

4. Thick Plates: whose internal stress condition resembles that of three dimensional continua.

In order to use plates as a resonant sensor, the geometrical configuration of the vibrating structure is preferred to be rectangular owing to their high rigidity and the directional sensitivity [117]. Choosing the plate material as titanium the ultrasonic sensor is designed and the fundamental frequency is evaluated with respect to the changes in thickness and aspect ratio. The aspect ratio of the plate is defined by the ratio of its length to the width. Using the closed form solution for a simply supported plate [120], the effect of varying the dimensions on frequency is observed as represented in Equation (39). The aspect ratio is varied in multiples of 2 from 2 to 10. The variation is shown in Figure 29.

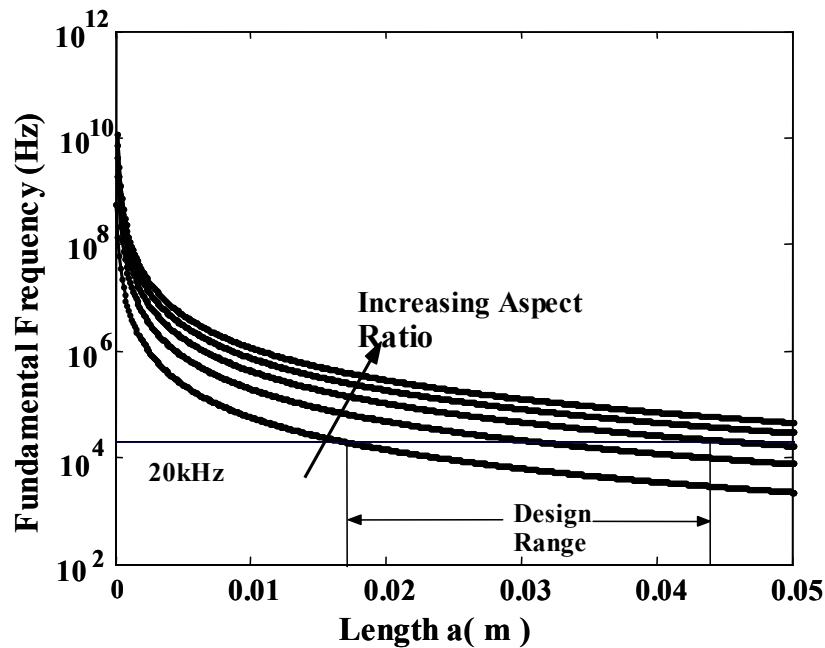


Figure 29 Effect of variation in natural frequency for various aspect ratios of the plate.

$$f_{ij} = \frac{\lambda_{ij}^2}{2\pi a^2} \left[\frac{Eh^3}{12\gamma(1-\nu^2)} \right]^{\frac{1}{2}} \quad (39)$$

A suitable design range for the dimensions of the sensor beam can be selected from Figure 29. To select a fundamental frequency of the vibrating plate above 20 kHz, a suitable length and a corresponding aspect ratio should be selected. If the width is selected as 0.005 m, a length of 0.04 m and an aspect ratio of 8 can be selected. All these simulations are carried out for a constant thickness. By fixing the aspect ratio and length, the appropriate thickness for the thin plate can be ascertained. By increasing the thickness the ultrasonic range can be achieved. The thickness is varied between 100 μm and 500 μm . Thus a suitable thickness of 450 μm yields a fundamental frequency above the ultrasonic range as shown in Figure 30.

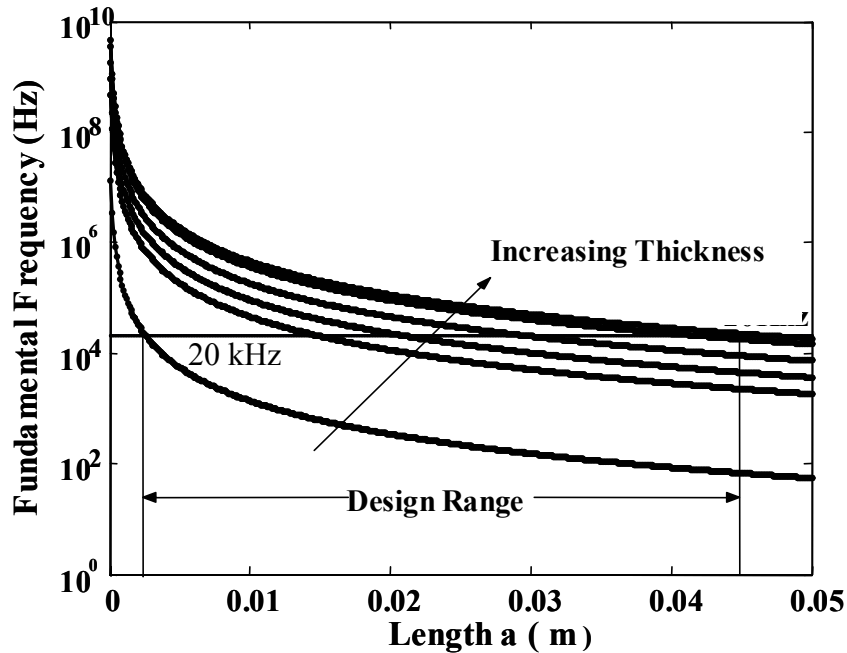


Figure 30 Effect of variation of thickness on the fundamental frequency of the plate.

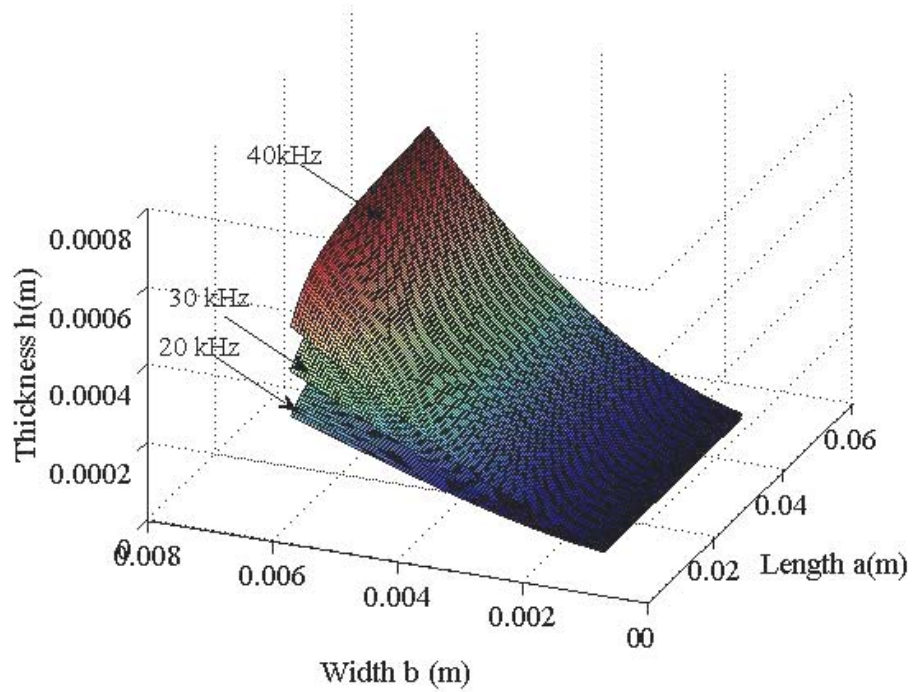


Figure 31 Generalized graph relating the resonant frequency and dimensions of the vibrating plate.

A generalized plot relating the dimensions of the plate for various frequencies is represented in Figure 31. Depending upon the chosen operational frequency range the dimension of the resonating micro-plate can be fixed from the generalized plot shown in Figure 31.

To complete the analysis, we also report the various mode shapes corresponding to the resonant sensor dimensions Figure 32. From published literature [120] we know that a general closed form solution does not exist for vibration of a rectangular plate with various elementary boundary conditions on each of the four edges.

However, it has been observed that the mode shapes of rectangular plates lying in the X-Y plane can be well approximated by a series of beam modes in the separable form of the variables as represented in Equation (40).

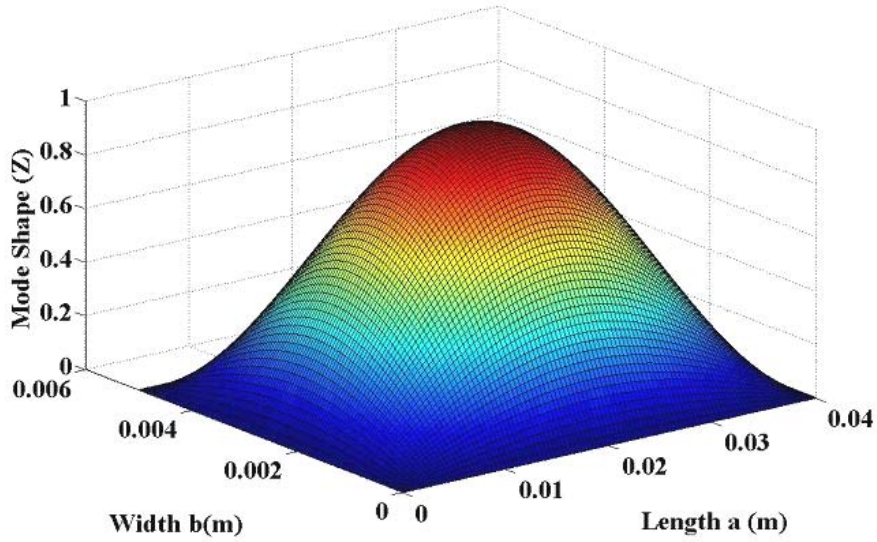


Figure 32 Mode shape (1, 1) of the vibrating plate having aspect ratio of 8.

$$\tilde{z}_{ij}(x, y) = \sum_m \sum_n \sin \frac{i\pi x}{a} \sin \frac{j\pi y}{b}, \quad i, j = 1, 2, 3, \dots \quad (40)$$

Hence, it can be observed that the quantifying the water loss during drying is possible by way of using ultrasound resonant sensors, wherein the sensor is resonated using ultrasound. Once the sensor is set into resonance and the drying process initiated, the change in mass brought about by drying can be related to a shift in the resonant frequency as shown above.

3.11 Conclusions

A linear relationship has been established between the dynamically varying quantities (mass and frequency) for a beam structure. It has also been shown that when the exciting frequency ω of ultrasound reaches the natural frequency ω_n of the fixed-fixed beam it goes into resonance which is illustrated in the frequency response plots. By extending the current beam model to a plate model issues related with sensitivity have been explored. The analysis shows that the real time monitoring of the water loss using ultrasound resonant sensors is possible. The

generalized graphs developed that relate the sensor dimensions with the natural frequency can be used as guides to select the appropriate size of the sensor that can result in the fundamental resonance frequency in the ultrasonic range.

CHAPTER 4. SUMMARY AND FUTURE WORK

The focus of the current study is to develop methods that would initiate the ambient temperature storage of Adipose Derived Adult Stem Cells. The experiments clearly indicate that these cells have the potential to be dehydrated and stored at ambient temperature without any special cryoprotective packaging to retain their growth and functionality. Drying protocols for such room temperature drying process and storage have been developed.

The effect of trehalose and glycerol in a saline media was observed to improve the functionality of the ASCs. The most efficacious methodology to preserve the ASCs is by drying them slowly and storing in vacuum sealed conditions. Observing and quantifying the effect of increasing the concentration of trehalose in an isotonic solution will be an important extension of the present study.

A theoretical approach to quantify the water loss during drying process has also been developed by considering a novel ultrasonic resonant sensor technique. Numerical studies have been carried out to develop the relationship between the change in the frequency to the change in mass during drying process using ultrasound resonant sensors. Analyses based on the beam and plate structure of the sensor have been carried out and numerical solutions for such sensor systems have been developed. Generalized plots relating the sensor dimensions and fundamental frequency are developed that can be used to select the sensors of appropriate dimensions that can give fundamental frequency in the ultrasound range. As an extension of the present work the sensors can be fabricated and experimental studies on the drying process can be carried out. A scheme for one possible experimental set up is proposed in Figure 32, where pulse-echo type ultrasonic system is used to vibrate a sensor containing the cell suspension sample.

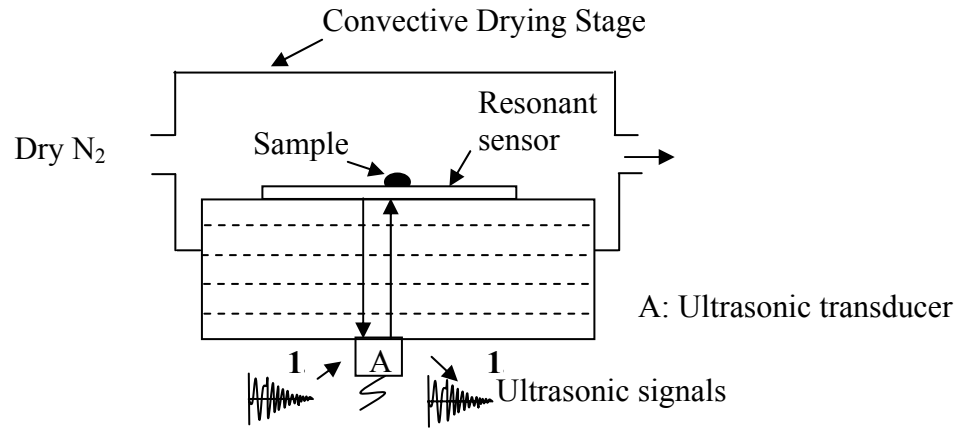


Figure 33 Proposed experimental set up.

The analytical model can be further refined by evaluating the effect on the fundamental frequency of vibration of the sensor, while considering the wave nature of ultrasonic waves. The sensitivity of the model can be increased by developing a frequency response function of the plate model.

REFERENCES

1. Zandstra, P. W., Nagy, A. "Stem Cell Bioengineering" *Annu. Rev. Biomed. Eng.* 3, 275-305 (2001).
2. Langer, R., Vacanti, J. P., "Tissue Engineering: the development of functional substitutes for damaged tissue" *Science* 260, 920-926 (1993).
3. Lagasse, E., Connors, H., Al-Dhalimy, M., Reitsma, M., Dohse, M., Osborne, L., Wang, X., Finegold, M., Weissman, I. L., Grompe, M. "Purified hematopoietic stem cells can differentiate into hepatocytes in vivo." *Nature Medicine* 6, 1229 - 1234 (2000).
4. "Life in Frozen State." edited by Fuller, B.J., Lane N., Benson, E.E. CRC Press, Boca Raton, Florida (2004).
5. Shalaev, E., Franks, F. "Changes in the Physical State of Model Mixtures During Freezing and Drying: Impact on Product Quality." *Cryobiology* 33, 14-26 (1996).
6. Mazur P. "Cryobiology: the freezing of biological systems" *Science* 168, 939-949 (1970).
7. Crowe L. M. "Lessons from nature: the role of sugars in anhydrobiosis." *Comp. Biochem. Phys. A* 131, 505-513 (2002).
8. Feofilova, E. P. "Deceleration of vital activity as a universal biochemical mechanism ensuring adaptation of microorganisms to stress factors." *A Review Appl. Biochem. Microbiol.* 39, 1-18 (2003).
9. Crowe, J. H., Hoekstra. F. A., Crowe, L. M. "Anhydrobiosis." *Annu. Rev. Physiol* 54, 579-599 (1992).
10. Van Gundy, S. D. "Factors in survival of Nematodes." *Ann. Rev. Phyopathol.* 3, 43-68 (1965).
11. Womersley, C. "A reevaluation of strategies employed by nematode anhydrobiotes in relation to their natural environment. In *Vistas on nematology*," J.A Veech and D.W.Dickinson (eds). Society on Nematologists, Hyattsville, Maryland, 165-173 (1987).
12. Perry, R. N. "Desiccation survival of parasitic nematodes." *Parasitology* 119, 819-830 (1999).
13. Crowe, J. H., Crowe, L. M. "Preservation of liposomes by freeze-drying" in *Liposome Technology* ed. Gregoriadis, G., Boca Raton, FL CRC Press. Second Ed, (1992)
14. Crowe, J. H., Crowe, L. M., Carpenter, J. F., Rudolph, A. S. "Interaction of sugars with membranes." *Biochim. Biophys Acta* 947, 367-384 (1988).
15. Keilin, D. "The Leeuwenhoek Lecture. The problem of anabiosis or latent life: history and current concepts." *Proc.R. Soc.Lond. B* 150, 149-191 (1959).

16. Caffrey, M., Fonseca, V., Leopold, C. "Lipid Sugar Interactions." *Plant Physiol.* 86, 754-758 (1988).
17. Green, J.L., Angell, C. A. "Phase relations and vitrification in saccharide water solutions and the trehalose anomaly." *J.Phys. Chem.* 93, 2880-2882 (1989).
18. Carpenter, J. F., Crowe, J. H., Crowe, L. H. "Comparisson of solute induced protein stabilization in aqueous solutions and in the frozen and dried states." *J. Dairy Sci.*, 73, 3627-3636 (1990).
19. Carpenter, J. F., Martin, B., Crowe, L. M., Crowe, J. H. "Stabilization of phosphofructokinase during air-drying with sugars and sugar/transition metal mixtures." *Cryobiology* 455-464 (1987).
20. Crowe, J. H., Crowe, L. M., Carpenter, J. F., Rudolph, A. S., Winstrom, C. A., Spargo, B. J., Anchrodogy, T. J. "Interactions of sugars with membranes." *Biochem. Biophys. Acta.* 947, 367-384 (1987).
21. Billi, D., Wright, D. J., Helm, R. F., Prickett, T., Potts, M., Crowe, J. H. "Engineering desiccation tolerance in E.Coli" *Appl. Environ. Microbiol.* 66(4), 1680-1684 (2000).
22. Leslie, S. B., Israeli, E., Lighthart, B., Crowe, L. M, Crowe, J. H. "Trehalose and Sucrose protect both membranes and proteins in intact bacteria during drying." *Appl. Environ. Microbiol.* 61, 3592-3597 (1995).
23. Crowe, J. H., Hoekstra, F. A., Crowe, L. M. "Membrane phase transitions are responsible for imbibitional damage in dry pollen." *Proc. Natl. Acad. Sci. USA.* 1989, 86, 520-523.
24. Crowe, J. H., Hoekstra, F. A., Crowe, L. M., Anchordoguy, T. J., Drobins, E. "Lipid phase transitions measured in intact cells with Fourier Transform Infrared Spectroscopy." *Cryobiology* 26, 76-84 (1989).
25. Brana, A. F., Manzanal, M. B., Hardisson, C., "Occurrence of polysaccharide granules in sporulating hyphae of *S. viridochromogenes*." *J Bacteriol.* 144(3), 1139-1142 (1980).
26. Brana, A. F., Mendez, C., Diaz, L. A., Manzanal, M. B., Hardisson, C. "Glycogen and trehalose accumulation during colony development in *Streptomyces antibioticus*." *J. Gen Microbiol.* 132, 1319-1326 (1986).
27. Miyamoto, Y., Imaizumi, T., Sukenhobe, J., Murakami, Y., Kawamura, S., Komatsu, Y. "Survival rate of microbes after freeze-drying and long term storage." *Cryobiology* 41, 251-255 (2000).
28. Madin, K. A. C., Crowe, J. H. "Anhydrobiosis in nematodes: carbohydrate and lipid metabolism during de-hydration." *J. Exp. Zool.* 193, 335-342 (1975).
29. Beker, M .J., Rapoport, A. I. "Conservation of yeasts by dehydration." *Adv. Biochem. Eng./Biotech.* 35,128-171 (1987)

30. Mille, Y., Girard, J. P., Beney, L., Gervais, P. "Air drying optimization of *Saccharomyces cerevisiae* through its water-glycerol dehydration properties." *J. Appl. Microbiol.* 99, 376-382 (2005).
31. Clegg, J. S. "Biochemical adaptations associated with the embryonic dormancy of *Artemia salina*." *Trans. Am. Microsc. Soc.* 93, 481-490 (1974).
32. Still, D. W., Kovach, D. A., Bradford, K. J. "Development of desiccation tolerance during embryogenesis in rice (*Oryza sativa*) and Wild rice (*Zizania palustris*)." *Plant Physiol.* 104, 431-438 (1994).
33. Blackman, S. A., Wettlaufer, S. H., Obendorf, R. L., Leopold, C. "Maturation proteins associated with desiccation tolerance in soybean." *Plant Physiol.* 96, 866-874 (1991).
34. Blackman, S. A., Obendorf, R. L., Leopold, C. "Maturation proteins and sugars in desiccation tolerance of developing soybean seeds." *Plant Physiol.* 100, 225-230 (1992).
35. Martinez, M. T., Ballester, A., Vieitez, A. M. "Cryopreservation of embryogenic cultures of *Quercus robur* using desiccation and vitrification procedures." *Cryobiology* 46, 182-189 (2003).
36. Eroglu, A., Toner, M., Toth, T. L. "Beneficial effect of microinjected trehalose on the cryosurvival of human oocytes." *Fertility and Sterility* 77, 152-158 (2002).
37. Beattie, G. M., Crowe, J. H., Lopez, A. D., Cirulli, V., Ricordi, C., Hayek, A. "Trehalose: a cryoprotectant that enhances recovery and preserves functions of human pancreatic islets after long term-storage." *Diabetes* 46, 519-523 (1997).
38. Bartels, A., Singh, M., Salamini, F. "Onset of desiccation tolerance during development of the barley embryo." *Planta* 175, 485-492 (1988).
39. Bruni, F., Leopold, C. "Glass Transition Temperature in Soybean." *Plant Physiol.* 96, 660-663 (1990).
40. Solomon, A., Ilan, P., Itamar, G. "Desiccation tolerance of *Muellerius cf. capillaries* (Nematoda: Protostronglidae) First Stage Larvae." *J. Parasitol.* 84 (4), 802-805 (1998).
41. Wolkers, W. F., Walker, N. J., Tablin, F., Crowe, J. H. "Human platelets loaded with trehalose survive free-drying." *Cryobiology* 42, 79-87 (2001).
42. Eroglu, A., Russo, M. J., Bieganski, R., Fowler, A., Cheley, S., Bayley, H., Toner, M. "Intracellular trehalose improves the survival of cryopreserved mammalian cells." *Nat. Biotech.* 163-181 (2000).
43. Aboagla, E. M. E., Terada, T. "Trehalose-enhanced fluidity of the goat sperm membrane and its protection during freezing." *Biol. Reprod.* 69, 1245-1250 (2003).

44. Buchanan, S. S., Gross, S. A., Acker J. P., Toner, M., Carpenter, J. F., Pyatt, D. W. "Cryopreservation of Stem Cells using trehalose: evaluation of the method using hematopoietic cell line." *Stem Cells Devel.* 13, 295-304 (2004).
45. Elbein, A. D., Pan, Y. T., Pastoszak, I., Carroll, D. "New Insights on trehalose: a multifunctional molecule." *Glycobiology* 13, 17R-27R (2003).
46. Bhowmick, P., Eroglu, A., Wright, D. L., Toner, M., Toth, T. L. "Osmotic behavior of mouse oocytes in the presence of different intracellular sugars." *Cryobiology* 45, 183-187 (2002).
47. Satpathy, G. R., Torok, Z., Bali, R., Dwyre, D. M., Little, E., Walker, N. J., Tablin, F., Crowe, J. H., Tsvetkova, N. M. "Loading red blood cells with trehalose: a step towards biostabilization." *Cryobiology* 49, 123-136 (2004).
48. Ward, M. A., Kaneko, T., Kusakabe, H., Biggers, J. D., Whittingham, D. G., Yanagimachi, R. "Long term storage preservation of mouse spermatozoa after freeze drying and freezing without cryoprotection." *Biol. Reprod.* 69, 2100-2108 (2003).
49. Guo, N., Puhlev, I., Brown, D. R., Mansbridge, J., Levine, F. "Trehalose expression confers desiccation tolerance on human cells." *Nat Biotech.* 18, 168-171 (2000).
50. Puhlev, I., Guo, N., Brown, D. R., Levine, F. "Desiccation tolerance in human cells." *Cryobiology* 42, 207-217 (2001).
51. Chen, T., Acker, J. P., Eroglu, A., Cheley, S., Bayley, H., Fowler, A., Toner, M. "Beneficial effect of intracellular trehalose on the membrane integrity of dried mammalian cells." *Cryobiology* 43, 168-181 (2001).
52. Gordon, S. L., Oppenheimer, S. R., Mackay, A. M., Brunnabend, J., Puhlev, I., Levine, F. "Recovery of human mesenchymal stem cells following dehydration and rehydration." *Cryobiology* 43, 182-187 (2001).
53. Matsuo, T. "Trehalose protects corneal epithelial cells from death by drying." *Br. J. Ophthalmol.* 85, 610-612(2005).
54. Ginnis, L. K., Zhu, L., Lawitts, J. A., Bhowmick, S., Toner, M., Biggers, J. D. "Mouse sperm desiccated and stored in trehalose medium without freezing." *Biol. Reprod.* 73, 627-633 (2005).
55. Becker, A., Scholeder, P., Steele, J. E., Wegener, G. "The regulation of trehalose metabolism in insects." *Experientia* 52, 433-439.
56. Crowe, J. H., Crowe, L. M., Jackson, S. A. "Preservation of structural and functional activity in lyophilized sarcoplasmic reticulum." *Arch. Biochem. Biophys.* 220, 477-484 (1983).

57. Crowe, J. H., Crowe, L. M., Carpenter, J. F., Rudolph, A.S., Wistrom, C A. "Stabilization of dry phospholipids bilayers and proteins by sugars." *Biochem. J.* 242, 1-10 (1987).
58. Crowe, J. H., Crowe, L. M., Hoekstra, F. A. "Phase transitions and permeability changes in dry membranes during rehydration." *J. Bioenerg. Biomembr.* 21, 77-91 (1989).
59. Pereira, C. S., Lins, R. D., Chandrashekhar, I., Freitas, L. C. G., Hunenberger, P. H. "Interaction of the disaccharide trehalose with a phospholipid bilayer: a molecular study." *Biophys. J.* 86, 2273-2285 (2004).
60. Clegg J. S., Seitz, P., Seitz, W., Hazlewood, C. F. "Cellular responses to extreme water loss: the water replacement hypothesis." *Cryobiology* 19, 306-316 (1982).
61. Carpenter, J. F., Crowe, J. F., "An infrared spectroscopic study of the interactions of carbohydrates with dried proteins." *Biochemistry* 28, 3916-3922.
62. Mouradian, R., Womersely, C., Crowe, L. M., Crowe, J. H. "Preservation of functional integrity during long term storage of a biological membrane." *Biochim. Biophys. Acta* 778, 615-617 (1984).
63. Sun, W. Q., Irving, T. C., Leopold A. C. "The role of sugar, vitrification and membrane phase-transition in seed desiccation tolerance." *Physiol. Plantarum* 90, 621-628 (1994).
64. Bhowmick, S., Zhu, L., McGinnis, L.; Lawitts, J., Nath, B. D., Toner, M.; Biggers, J. D. "Desiccation tolerance of spermatozoa dried at ambient temperature: Production of Fetal Mice." *Biol. Reprod.* 68, 1779-1786 (2003).
65. Ma, X. C., Jamil, K., MacRae, T. H., Clegg, J. S., Russell, J. M., Villeneuve, T. S., Euloth, M., Sun, Y., Crowe, J. H., Tablin, F., Oliver. A. E. "A small stress protein acts synergistically with trehalose to confer desiccation tolerance on mammalian cells." *Cryobiology* 51, 15-28 (2005).
66. Thundat, T., Warmack, R. J., Chen, G. Y., Allison, D. P. "Thermal and ambient-induced scanning force microscope." *Appl. Phys. Lett.* 64, 2894-2896 (1994).
67. Fritz, J., Baller, M. K., Lang, H. P., Rothuizen, H., Vettiger, P., Meyer, E., Guntherodt, H. J., Gerber, C., Gimzewski, K., "Translating biomolecular recognition into nanomechanics." *Science* 288, 316-318 (2000).
68. Green, J. B. D., Lee, G. U. "Atomic Force Microscopy with Patterened Cantilevers and Tip Arrays." *Langmuir* 16, 4009-4015 (2000).
69. Binnig, G., Quate, C.F., Gerber, C. "Atomic Force Microscope." *Phys. Rev. Lett.* 56, 930-933 (1986).
70. Saris, D. "Scanning Force Microscopy" Oxford University Press, New York (1994).

71. Ilic, B., Czaplewski, M., Zalalutdinov, M., Craighead, H. G., Neuzil, P., Campagnolo, C., Batt, C. "Single cell detection with micromechanical oscillators." *J.Vac. Sci. Technol. B* 19, 2825-2828 (2001).
72. Ferrari, V., Mariolo, D., Taroni, A. "Theory and modeling and characterization of PZT-on-alumina resonant piezo-layers as acoustic wave mass sensors" *Sensors and Actuators A* 92, 182-190 (2001).
73. Elwenspoek, M., Wiegerink, R. "Mechanical Microsensors." Series: Microtechnology and MEMS Springer, Verlag Publications, (2001)
74. Palikala, V. K. "Design of an ultrasonic strain sensor." M.S. Thesis, Mechanical Engineering Department, Louisiana State University, Baton Rouge, LA (1997).
75. Schomburg, W. K., Vitt, M., Bacher, W., Borner, M. W., Menz, W. "Measurements of Physical parameters with Ultrasound and Microdiaphragms" *IEEE Proceedings of Micro Electromechanical Systems 1995 (MEMS'95)*, pg. 139-145.
76. Ode, P.I. "Gravimetric sensing of metallic deposits using an end loaded microfabricated beam structure." *Sensors and Actuators B* 53, 191-196 (1998).
77. Maute, M., Raibe, S., Prins, F. E., Kern, D. P., Ulmer, H., Gopel, W. W. "Detection of volatile organic compounds (VOCs) with polymer coated cantilevers." *Sensors and Actuators B* 58, 505-511 (1999).
78. Suda, T., Nagata, S. "Why do defects in the Fas-Fas Ligand system cause autoimmunity?" *J. Allergy Clin. Immunol.*, 97-101 (1997).
79. Toma, J. G., Akhavan, M., Feranandes, K. J. "Isolation of multipotent adult stem cells from the dermis of mammalian skin." *Nat. Cell Biol.* 3, 778-784 (2001).
80. Burt, R. K., Marmont, M. "Stem Cell Therapy for Autoimmune Disease." Landes Bioscience, Georgetown, TX, Chapter 2 (2004).
81. Sen, A., Lea-Currie, Y. R., Sujkowska, D., Franklin, D. M., Wilkison, W. O., Halvorsen, Y. D., Gimble, J. M. "Adipogenic potential of human adipose derived stromal cells from multiple donors is heterogeneous." *J. Cell Biochem.*, 81, 312-319 (2001).
82. Halvorsen, Y. D. C., Franklin, D., Bond, A. L., Hitt, D. C., Auchter, C., Boskey, A. L., Paschalis, E. P., Wilkison, W. O., Gimble, J. M. "Extracellular matrix mineralization and osteoblast gene expression by human adipose tissue-derived stromal cells." *Tissue Eng.* 7, 729-741 (2001).
83. Zuk, P. A., Zhu, M., Mizuno, H., Huang, J. I., Futrell, W. J., Katz, A. J., Benhaim, P., Lorenz, H. P., Hedrick, M. H. "Multi-lineage cells from human adipose tissue: implications for cell-based therapies." *Tissue Eng.* 7, 211-226 (2001).

84. Gimble, J. M., Guilak, F. "Adipose-derived adult stem cells: isolation, characterization, and differentiation potential." *Cytotherapy* 5, 362-369 (2003).
85. Thirumala, S., Zvonic, S., Floyd, E., Gimble J. M., Devireddy R.V. "The Effect of Various Freezing Parameters on the Immediate Post-Thaw Membrane Integrity of Adipose Tissue Derived Adult Stem Cells." *Biotechnology Progress* 21, 1511-1524 (2005).
86. Awad, H. A., Wickham, M. Q., Leddy, H. A., Gimble, J. M., Guilak, F. "Chondrogenic differentiation of adipose-derived adult stem cells in agarose, alginate, and gelatin scaffolds." *Biomaterials* 25, 3211-3222 (2004).
87. Mizuno, H., Zuk, P. A., Zhu, M., Lorenz, H. P., Benhaim, P., Hedrick, M. H. "Myogenic differentiation of human processed lipoaspirate cells." *Plastic Reconstr. Surg.* 109, 199–209 (2001).
88. Wickham, M. Q., Erickson, G. R., Gimble, J. M., Vail, T. P., Guilak, F. "Multipotent stromal cells derived from the infrapatellar fat pad of the knee." *Clin. Orthop.* 412, 196-212 (2003).
89. Gimble, J. M., Nuttall, M. E. "Bone and Fat: Old Questions, New Insights." *Endocrine* 23, 183-188 (2004).
90. Safford, K. M., Hicok, K. C., Safford, S. D., Halvorsen, Y. D., Wilkison, W. O., Gimble J. M., Rice, H. E. "Neurogenic differentiation of murine and human adipose-derived stromal cells." *Biochem. Biophys. Res. Commun.* 294, 371-379 (2002).
91. Ashjian, P. H., Elbarbary, A. S., Edmonds, B., DeUgarte, D., Zhu, M., Zuk, P. A., Lorenz, H. P., Benhaim, P., Hedrick, M. H. "In vitro differentiation of human processed lipoaspirate cells into early neural progenitors." *Plastic Reconstr. Surg.* 111, 1922-1931 (2003).
92. Safford, K. M., Safford, S. D., Gimble, J. M., Shetty, A. K., Rice, H. E. "Characterization of neuronal/glial differentiation of murine adipose-derived adult stromal cells." *Exp Neurol.* 187, 319-328 (2004).
93. Lendeckel, S., Jodicke, A., Christophis, P., Heidinger, K., Wolff, J., Fraser, J. K., Hedrick, M. H., Berthold, L., Howaldt, H. P. "Autologous stem cells (adipose) and fibrin glue used to treat widespread traumatic calvarial defects: case report." *J Craniomaxillofac Surg.* 32, 370-373 (2004).
94. Hicok, K., du Laney, T., Sheng Zhou, Y., Halvorsen, Y. D. C., Hitt, C. D, Cooper, L. F., Gimble, J. M. "Human Adipose Derived Adult Stem Cells Produce Osteoid In Vivo." *Tissue Eng.* 10, 371-380 (2004).
95. Guilak, F., Lott, K. E., Awad, H. A., Cao, Q., Hicok, K. C., Fermor, B., Gimble, J. M. "Clonal analysis of the differentiation potential of human adipose-derived adult stem cells." *J. Cell Physiol.* 2005, InPress

96. Barnes, D. W. H., Loutit, J. F. "The radiation recovery factor: Preservation by the Polge–Smith–Parkes technique." *J. Natl. Cancer Inst.* 15, 901 (1955).
97. English, D., Paterson, A. H., Bone, G., McPherson, T. A. "Cryopreservation of canine hematopoietic cells." *Clin. Invest. Med.* 2, 67–74 (1979).
98. Jackson, J., Kloster, T., Welniak, L., Damon, M., Rehder, B., Schmechel, B., Ward, B., Kessinger, A. "Peripheral blood-derived stem cells can be successfully cryopreserved without using controlled-rate freezing." *Prog. Clin. Biol. Res.* 377, 367–371 (1992).
99. Chen, Q., Haddad, G. G. "Role of Trehalose Phosphate Synthase and Trehalose during Hypoxia: From Flies to Mammals." *J Expt Biol* 207, 3125-3129 (2004).
100. Huang, Z., Tunnacliffe, A. "Response of Human Cells to Desiccation: Comparison with Hyperosmotic Stress Response." *J Physiol* 558, 181-191 (2004).
101. Crowe, J. H., Crowe, L. M., Carpenter, J. F. "Preserving Dry Biomaterials: The Water Replacement Hypothesis. *Biopharm* 6, 40-43 (1993).
102. Russo, M. J., Bayley, H., Toner, M. "Reversible Permeabilization of Plasma Membranes with an Engineered Switchable Pore." *Nat Biotech* 15, 278-282 (1997).
103. Erdag G., Eroglu A., Morgan J. R., Toner M. "Cryopreservation of Fetal Skin is Improved by Extracellular Trehalose." *Cryobiology* 44, 218-228 (2002).
104. Kempf, B., Bremer, E. "Uptake and Synthesis of Compatible Solutes as Microbial Stress Responses to High Osmolality Environments." *Arch Microbiol*, 170, 319-330 (1998).
105. Hohmann, S. "Osmotic Stress Signaling and Osmoadaptation in Yeasts." *Microbiol Mol Biol Rev* 66, 300-372 (2002)
106. Räsänen, L. A., Saijets, S., Jokinen, K., Lindström, K. "Evaluation of the Roles of Two Compatible Solutes, Glycine Betaine and Trehalose, for the *Acacia senegal*–*Sinorhizobium* Symbiosis Exposed to Drought Stress." *Plant Soil* 260, 237-251 (2004).
107. Acker, J. P., Fowler, A., Lauman, B., Cheley, S., Toner, M. "Survival of Desiccated Mammalian Cells: Beneficial Effects of Isotonic Media." *Cell Preservation Technology* 1, 129-140 (2002).
108. Wesley-Smith, J., Pammenter, N. W., Berjak, P., Walters, C. "The Effects of Two Drying Rates on the Desiccation Tolerance of Embryonic Axes of Recalcitrant Jackfruit (*Artocarpus heterophyllus* Lamk.) Seeds." *Ann Bot*, 88, 653-664 (2001).
109. Leach, R. H., Scott, W. J. "The influence of rehydration on the viability of dried microorganisms." *J Gen Microbiol* 21, 295-307 (1959).
110. Mille, Y., Beney, L., Gervais, P. "Magnitude and Kinetics of Rehydration Influence the Viability of Dehydrated *E. coli* K-12." *Biotech Bioeng* 83, 578-582 (2003).

111. Beney, L., Mille, Y., Gervais, P. "Death of Escherichia coli during rapid and severe dehydration is related to lipid phase transition." *Appl. Microbiol. Biotech.* 65, 457-464 (2004).
112. Vollmer, F., Braun, D., Libchaber, A., Khoshshima, M., Teraoka, I., Arnold, S. "Protein detection by optical shift of a resonant microcavity." *Applied Physics Letters*, 80 (21), 4057-4059 (2002).
113. Kinnell, P. K., Ward, M. C., Craddock, R. "Physical characterisation of selective stress coupling for resonant pressure sensors" *Sensors and Actuators A*, 115, 230-234 (2004).
114. Guan, S. "Frequency encoding of resonant mass sensors for chemical vapor detection." *Analytical Chemistry* 75, 4551-4557 (2003).
115. Gaidarzhy, A., Zolfagharkhani, G., Badzey, R. L., Mohanty, P. "Spectral response of a gigahertz-range nanomechanical oscillator." *Applied Physics Letters* 86, 254103-1-254103-3 (2005)
116. Ong, K. G., Puckett, L. G., Sharma, B. V., Loiselle, M., Grimes, C. A., Bachas, L. G. "Wireless passive resonant-circuit sensors for monitoring food quality." *Proceedings of SPIE- The International Society for Optical Engineering*, 4575, 150-159 (2002).
117. Majkut, F. "Analysis Design, and test of a passive ultrasonic stress sensor." M.S. Thesis, Mechanical Engineering Department, Louisiana State University, Baton Rouge, LA (1999).
118. Schomburg, W. K., Vitt, M., Bacher, W., Borner, M., Menz, W. "Measurements of physical parameters using ultrasound and microdiaphragms." *Proceedings of the IEEE Micro Electro Mechanical Systems Workshop*, 139-144 (1995).
119. Meirovitch, L. "Fundamental of vibrations." McGraw Hill, NY, Ed (2001)
120. Blevins, R. D. "Formulas for natural frequency and mode shape." Litton Educational Publishing, NY Inc Ed (1979).
121. Yang, W. H. "A method for eigenvalues of the sparse λ -matrices." *Int. J. Numeric. Meth. in Eng.* 19,943-948 (1983).
122. Singh, K. V., Ram, Y. "Transcendental eigenvalue problem and its applications." *AIAA Journal* 40, 1402-1407 (2002)
123. Low, K. H. "A comparative study of the eigenvalue solutions for mass-loaded beams under classical boundary conditions." *International Journal of Mechanical Sciences* 43, 237-244 (2001)
124. Rao, S. S. "Mechanical Vibrations" Reading, MA: Addison-Wesley Boston MA, (1995).
125. Elmore, W. C., Heald, M. A. "Physics of Waves" McGraw Hill Company, NY (1969).

APPENDIX: TRANSCENDENTAL EIGENVALUE MATRICES

Matrix A

$$\begin{bmatrix}
 0 & 1 & 0 & 1 & 0 & 0 & 0 & 0 \\
 1 & 0 & 1 & 0 & 0 & 0 & 0 & 0 \\
 \sin \lambda\alpha & \cos \lambda\alpha & \sinh \lambda\alpha & \cosh \lambda\alpha & -\sin \lambda\alpha & -\cos \lambda\alpha & -\sinh \lambda\alpha & -\cosh \lambda\alpha \\
 \lambda \cos \lambda\alpha & -\lambda \sin \lambda\alpha & \lambda \cosh \lambda\alpha & \lambda \sinh \lambda\alpha & -\lambda \cos \lambda\alpha & \lambda \sin \lambda\alpha & -\lambda \cosh \lambda\alpha & -\lambda \sinh \lambda\alpha \\
 -\lambda^2 \sin \lambda\alpha & -\lambda^2 \cos \lambda\alpha & \lambda^2 \sinh \lambda\alpha & \lambda^2 \cosh \lambda\alpha & \lambda^2 \sin \lambda\alpha & \lambda^2 \cos \lambda\alpha & -\lambda^2 \sinh \lambda\alpha & -\lambda^2 \cosh \lambda\alpha \\
 \begin{pmatrix} -\lambda^3 \cos \lambda\alpha \\ +\beta\lambda^4 \sin \lambda\alpha \end{pmatrix} & \begin{pmatrix} \lambda^3 \sin \lambda\alpha \\ +\beta\lambda^4 \cos \lambda\alpha \end{pmatrix} & \begin{pmatrix} \lambda^3 \cosh \lambda\alpha \\ +\beta\lambda^4 \sinh \lambda\alpha \end{pmatrix} & \begin{pmatrix} \lambda^3 \sinh \lambda\alpha \\ +\beta\lambda^4 \cosh \lambda\alpha \end{pmatrix} & \lambda^3 \cos \lambda\alpha & -\lambda^3 \sin \lambda\alpha & -\lambda^3 \cosh \lambda\alpha & -\lambda^3 \sinh \lambda\alpha \\
 0 & 0 & 0 & 0 & \sin \lambda\alpha & \cos \lambda\alpha & \sinh \lambda\alpha & \cosh \lambda\alpha \\
 0 & 0 & 0 & 0 & \cos \lambda\alpha & -\sin \lambda\alpha & \cosh \lambda\alpha & \sinh \lambda\alpha
 \end{bmatrix}$$

Matrix B

$$\begin{bmatrix}
 0 & 0 & 0 & 0 & 0 & 0 & 0 & 0 \\
 0 & 0 & 0 & 0 & 0 & 0 & 0 & 0 \\
 \begin{pmatrix} \alpha \cos \lambda\alpha \\ \cos \lambda\alpha \\ -\lambda\alpha \sin \lambda\alpha \end{pmatrix} & -\begin{pmatrix} \alpha \sin \lambda\alpha \\ \sin \lambda\alpha \\ +\lambda\alpha \cos \lambda\alpha \end{pmatrix} & \begin{pmatrix} \alpha \cosh \lambda\alpha \\ \cosh \lambda\alpha \\ +\lambda\alpha \sinh \lambda\alpha \end{pmatrix} & \begin{pmatrix} \alpha \sinh \lambda\alpha \\ \sinh \lambda\alpha \\ +\lambda\alpha \cosh \lambda\alpha \end{pmatrix} & -\begin{pmatrix} \alpha \cos \lambda\alpha \\ -\cos \lambda\alpha \\ +\lambda\alpha \sin \lambda\alpha \end{pmatrix} & \begin{pmatrix} \alpha \sin \lambda\alpha \\ \sin \lambda\alpha \\ +\lambda\alpha \cos \lambda\alpha \end{pmatrix} & -\begin{pmatrix} \alpha \cosh \lambda\alpha \\ \cosh \lambda\alpha \\ +\lambda\alpha \sinh \lambda\alpha \end{pmatrix} & -\begin{pmatrix} \alpha \sinh \lambda\alpha \\ \sinh \lambda\alpha \\ +\lambda\alpha \cosh \lambda\alpha \end{pmatrix} \\
 \begin{pmatrix} -2\lambda \sin \lambda\alpha \\ -\lambda^3 \alpha \cos \lambda\alpha \end{pmatrix} & -\begin{pmatrix} 2\lambda \cos \lambda\alpha \\ -\lambda^3 \alpha \sin \lambda\alpha \end{pmatrix} & \begin{pmatrix} 2\lambda \sinh \lambda\alpha \\ +\lambda^3 \cosh \lambda\alpha \end{pmatrix} & \begin{pmatrix} 2\lambda \cosh \lambda\alpha \\ +\lambda^3 \sinh \lambda\alpha \end{pmatrix} & \begin{pmatrix} 2\lambda \sin \lambda\alpha \\ +\lambda^3 \alpha \cos \lambda\alpha \end{pmatrix} & \begin{pmatrix} 2\lambda \cos \lambda\alpha \\ +\lambda^3 \alpha \sin \lambda\alpha \end{pmatrix} & -\begin{pmatrix} 2\lambda \sinh \lambda\alpha \\ +\lambda^3 \alpha \cosh \lambda\alpha \end{pmatrix} & \begin{pmatrix} 2\lambda \cosh \lambda\alpha \\ +\lambda^3 \alpha \sinh \lambda\alpha \end{pmatrix} \\
 -\begin{pmatrix} 3\lambda^2 \cos \lambda\alpha \\ -\lambda^3 \alpha \sin \lambda\alpha \end{pmatrix} & \begin{pmatrix} 3\lambda^2 \sin \lambda\alpha \\ +\lambda^3 \alpha \cos \lambda\alpha \end{pmatrix} & \begin{pmatrix} 3\lambda^2 \cosh \lambda\alpha \\ +\lambda^3 \alpha \sinh \lambda\alpha \end{pmatrix} & \begin{pmatrix} 3\lambda^2 \sinh \lambda\alpha \\ +\lambda^3 \alpha \cosh \lambda\alpha \end{pmatrix} & \begin{pmatrix} 3\lambda^2 \cos \lambda\alpha \\ -\lambda^3 \alpha \sin \lambda\alpha \end{pmatrix} & -\begin{pmatrix} 3\lambda^2 \sin \lambda\alpha \\ +\lambda^3 \alpha \cos \lambda\alpha \end{pmatrix} & -\begin{pmatrix} 3\lambda^2 \cosh \lambda\alpha \\ +\lambda^3 \alpha \sinh \lambda\alpha \end{pmatrix} & -\begin{pmatrix} 3\lambda^2 \sinh \lambda\alpha \\ +\lambda^3 \alpha \cosh \lambda\alpha \end{pmatrix} \\
 +\begin{pmatrix} 4\beta\lambda^3 \sin \lambda\alpha \\ +\beta\lambda^4 \alpha \cos \lambda\alpha \end{pmatrix} & +\begin{pmatrix} 4\beta\lambda^3 \cos \lambda\alpha \\ -\beta\lambda^4 \alpha \sin \lambda\alpha \end{pmatrix} & +\begin{pmatrix} 4\beta\lambda^3 \sinh \lambda\alpha \\ +\beta\lambda^4 \alpha \cosh \lambda\alpha \end{pmatrix} & +\begin{pmatrix} 4\beta\lambda^3 \cosh \lambda\alpha \\ +\beta\lambda^4 \alpha \sinh \lambda\alpha \end{pmatrix} & \begin{pmatrix} \alpha \cos \lambda\alpha \\ -\alpha \sin \lambda\alpha \end{pmatrix} & \begin{pmatrix} \alpha \sin \lambda\alpha \\ -\alpha \cos \lambda\alpha \end{pmatrix} & \begin{pmatrix} \alpha \cosh \lambda\alpha \\ \alpha \sinh \lambda\alpha \end{pmatrix} & \begin{pmatrix} \alpha \sinh \lambda\alpha \\ \alpha \cosh \lambda\alpha \end{pmatrix} \\
 0 & 0 & 0 & 0 & \alpha \cos \lambda\alpha & -\alpha \sin \lambda\alpha & \alpha \cosh \lambda\alpha & \alpha \sinh \lambda\alpha \\
 0 & 0 & 0 & 0 & -\alpha \sin \lambda\alpha & -\alpha \cos \lambda\alpha & \alpha \sinh \lambda\alpha & \alpha \cosh \lambda\alpha
 \end{bmatrix}$$

VITA

Surbhi Mittal was born in Thiruvananthapuram, Kerala, India, in May 1979. She completed her high school studies and joined the undergraduate program in the Department of Mechanical Engineering at SCT College of Engineering, Kerala University, India, in 1997. She graduated with the degree of Bachelor of Technology in 2001, with honors. Surbhi joined Louisiana State University, Baton Rouge, to pursue a master's program and expects to receive that degree in mechanical engineering at the December 2005 commencement. She is the recipient of the Blue Ribbon Award – 2004 from the Materials Research Society for her research work related to design of resonant ultrasound sensors.